Fundamentals of SAR applied to Environmental Monitoring

Dr. Polyanna da Conceição Bispo
polyanna.bispo@manchester.ac.uk
Twitter: @polybispo @rsategroup

Lecture 4

Intended learning outcomes

- Geometric proprieties including SAR image interpretation and slant-range distortions
- What SAR Backscattering is
- Types of backscattering mechanisms
- SAR backscatter in forests and applications

## Geometric proprieties: SAR image interpretation and slant-range distortions

While the images created by SAR can be rendered into a recognizable terrain map, there are important differences between optical imagery and SAR imagery. SAR imagery is considered a non-literal imagery type because it does not look like an optical image which is generally intuitive to humans. These aspects must be understood for accurate image interpretation to be performed.
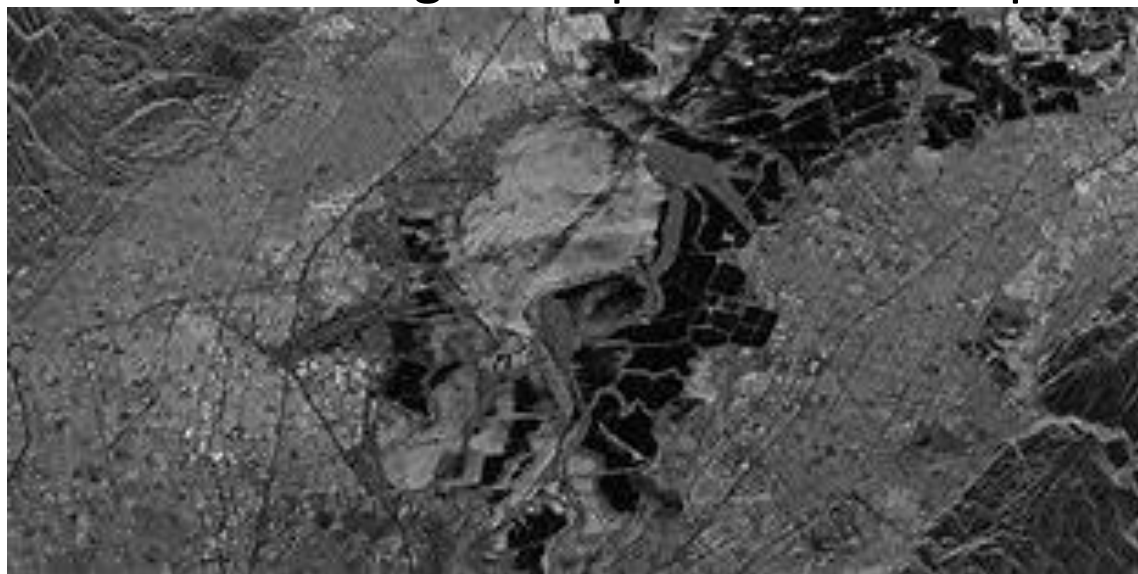
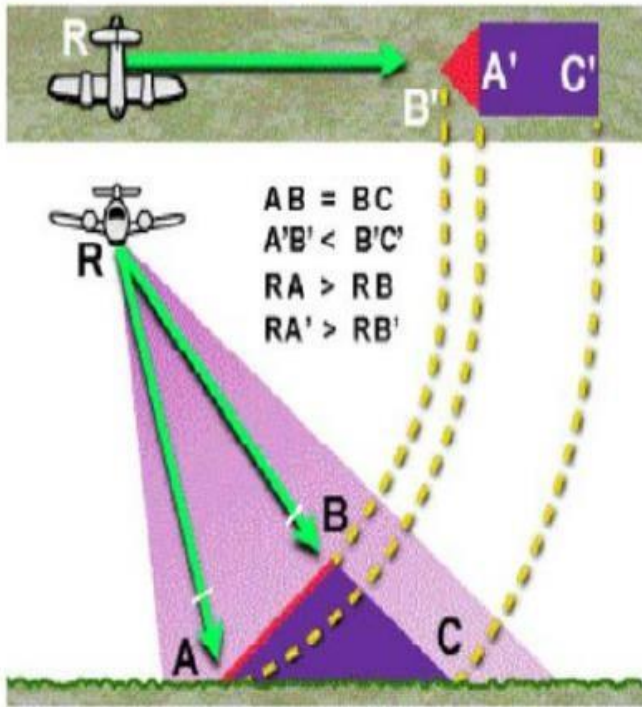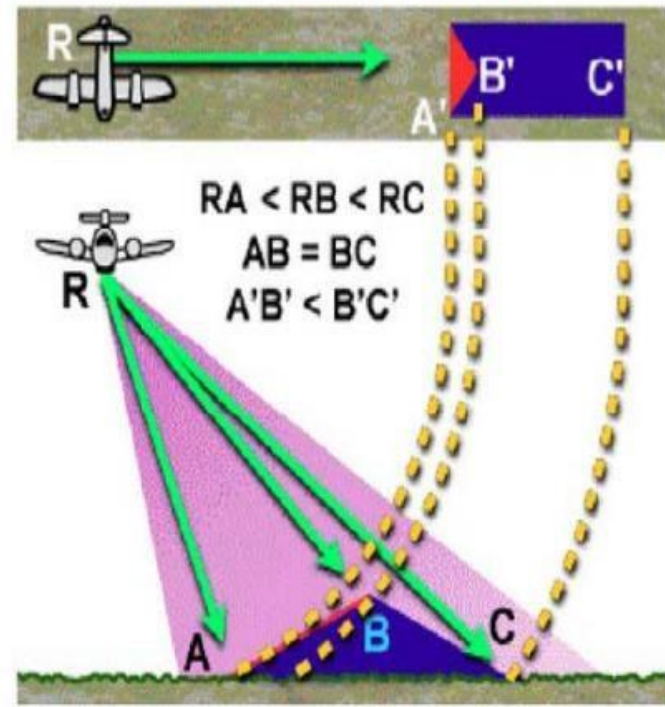# Slant Range Distortions
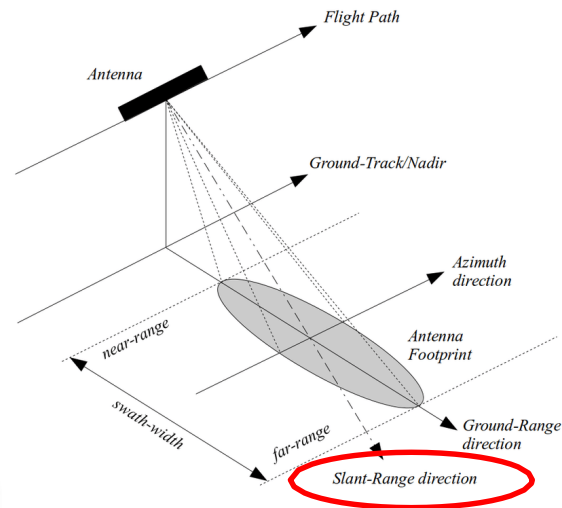
Slant Range

Ground Range

Source: Erika Podest, Basics of SAR: ARSET Applied Remote Sensing Training
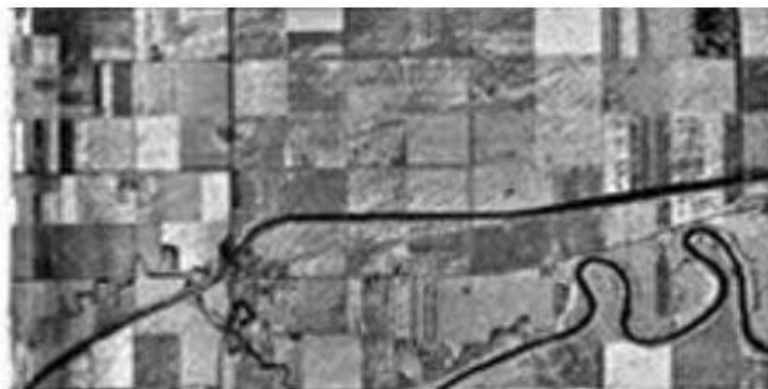
Geometric Distortion

Layover

$AB = BC$
$A'B' < B'C'$
$RA > RB$
$RA' > RB'$

Foreshortening

$RA < RB < RC$
$AB = BC$
$A'B' < B'C'$

Source: Natural Resources Canada

Source: Erika Podest, Basics of SAR: NASA-ARSET Applied Remote Sensing Training

Foreshortening

Before Correction
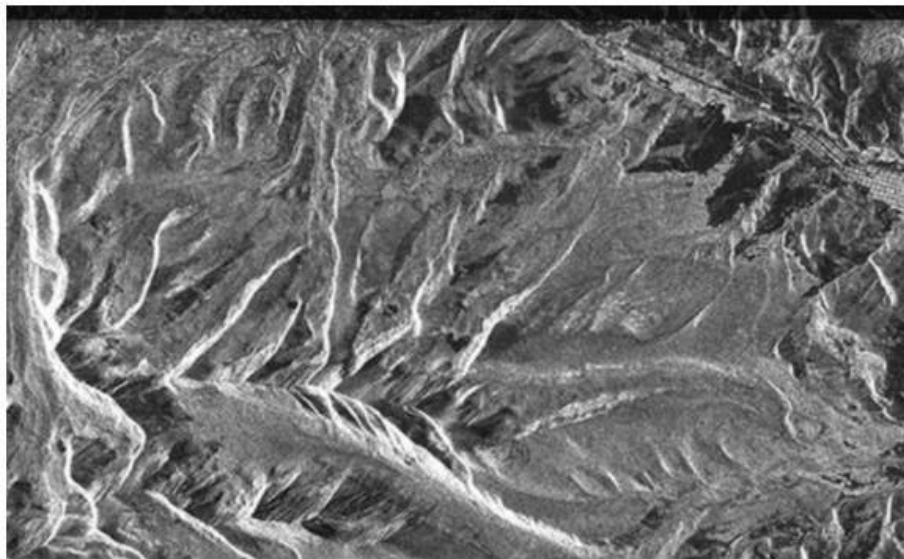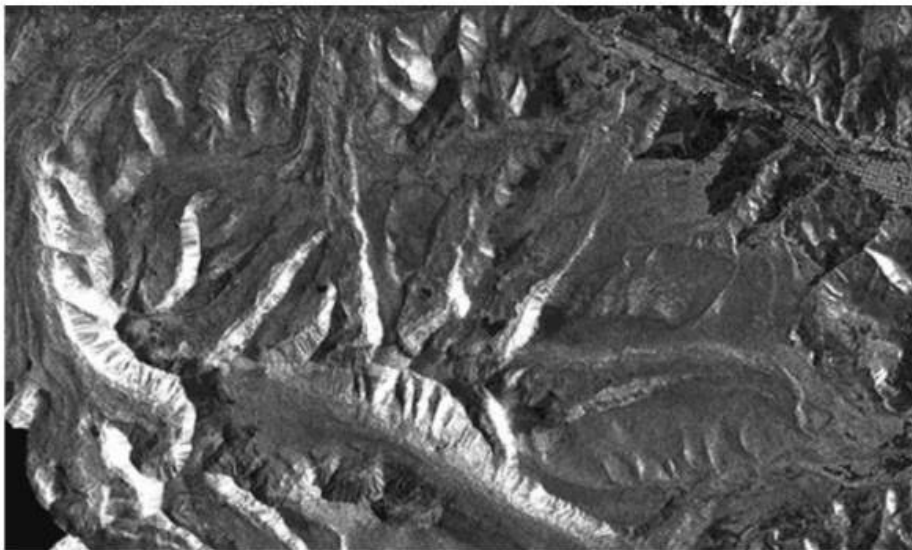
After Correction

Shadow

Source: Natural Resources Canada

Radiometric Distortion

- The user must correct for the influence of topography on backscatter
- This correction eliminates high values in areas of complex topography
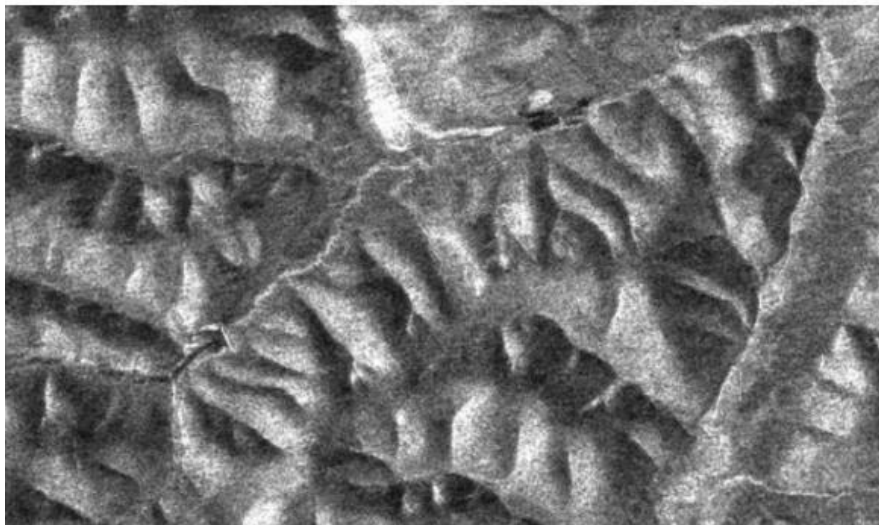
Before Correction   After Correction

Image Credits: ASF

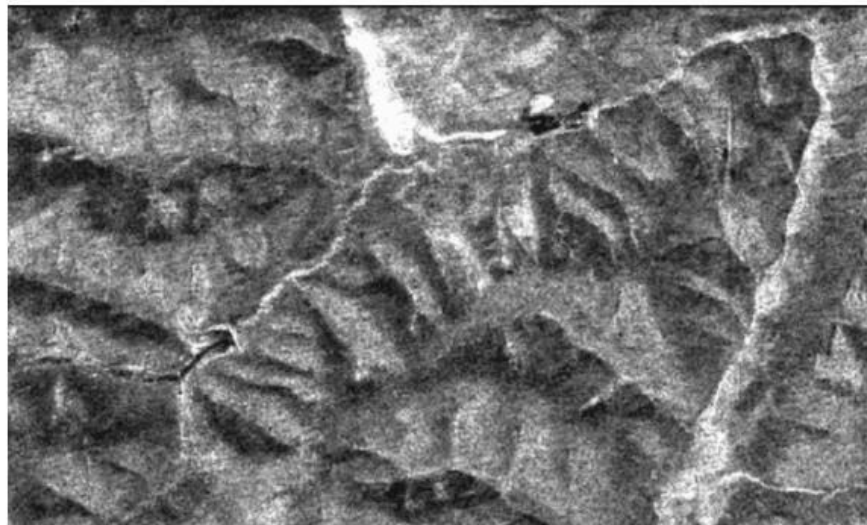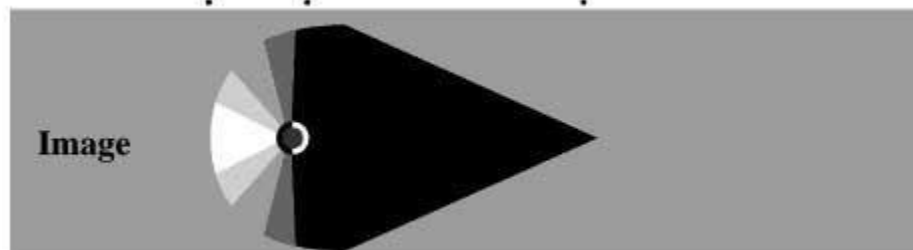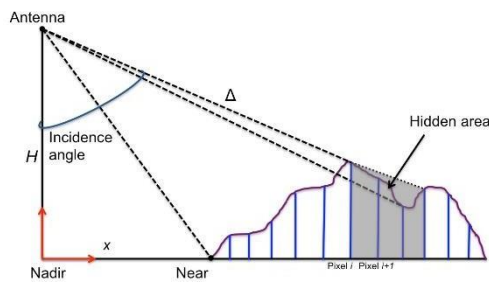**Source:** Erika Podest, Basics of SAR: ARSET Applied Remote Sensing Training

Shadowing

Shadowing is caused for the same reasons that shadows are formed in optical imagery: an object blocks the path of direct radiation — visible light in the case of optical imaging and the radar beam in the case of SAR. However, unlike optical imagery in which objects in shadows can be seen due to atmospheric scattering, there is no information in a SAR shadow because there is no return signal

SHADOW

- Area behind mountain cannot be seen by sensor
- Shadow effects *increase* with increasing look angle

radar shadow

ground range

Antenna

Incidence angle

H

x

Nadir   Near

Δ

Hidden area

Pixel i Pixel i+1

Shadow

Distortion
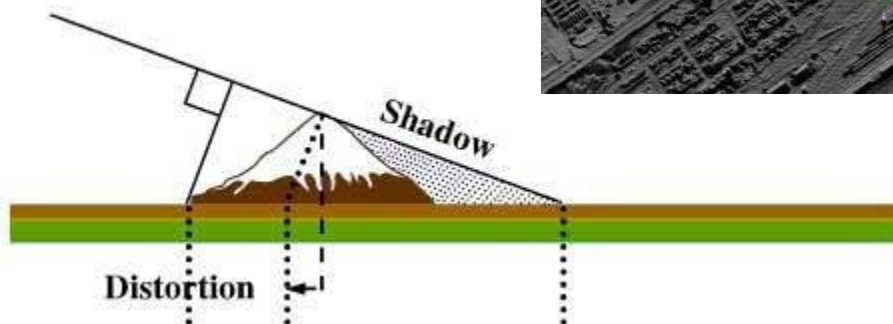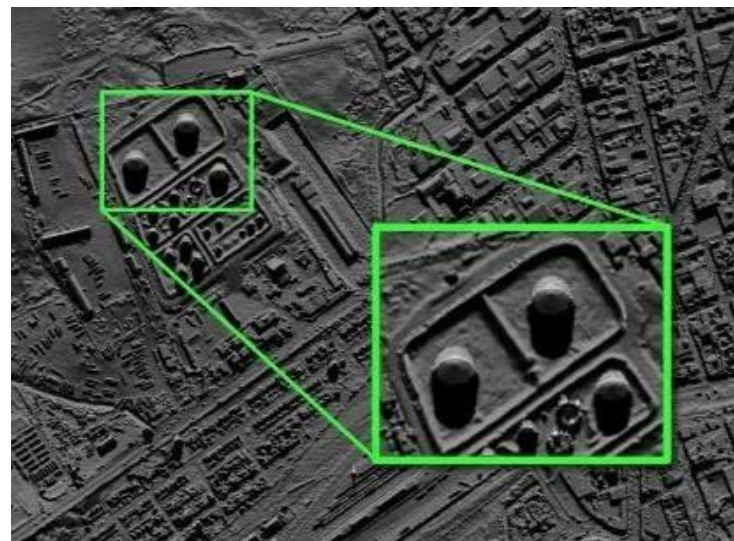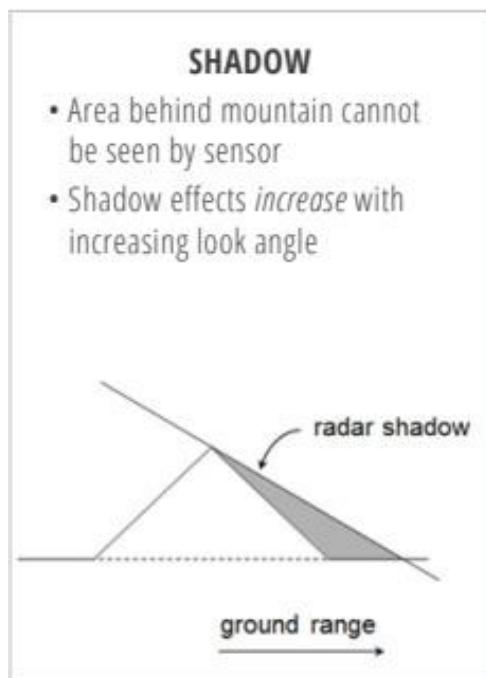
Image

Foreshortening

Because SAR is a side-looking, ranging instrument, the backscattered returns will be arranged in the image based on how far the target is from the antenna along the slant plane (radar-image plane). This causes some interesting geometrical distortions in the imagery, such as foreshortening.
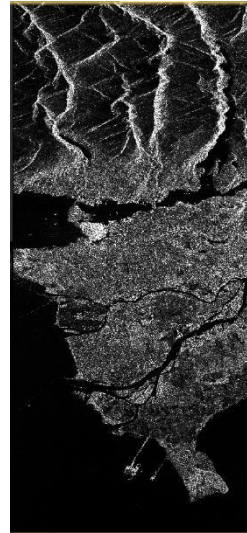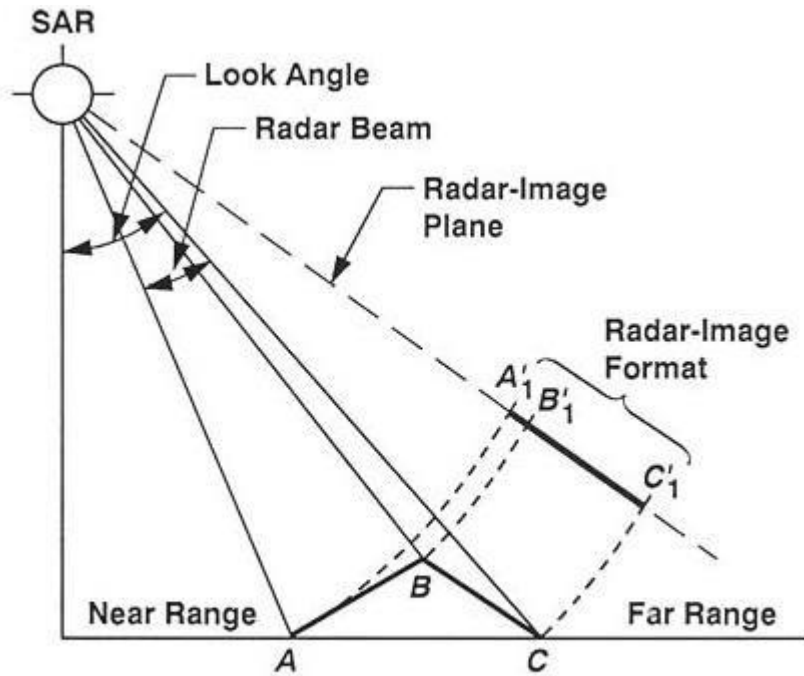
- 'shortening' of slopes facing the radar

- 'stretching' of slopes oppositely oriented to the radar

FORESHORTENING
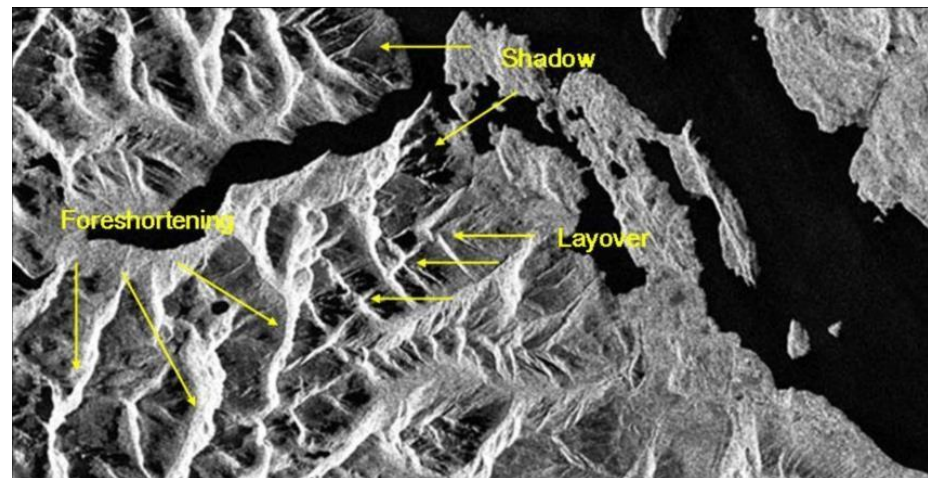- Sensor-facing slope foreshortened in image
- Foreshortening effects *decrease* with increasing look angle
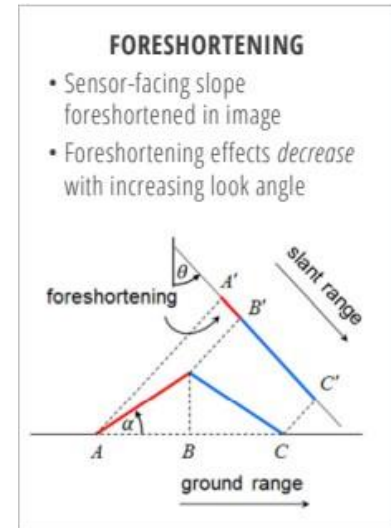
Figure 4. Foreshortening Geometry (Credit: NASA)

Layover

Layover is an extreme example of foreshortening where the object is so tall that the radar signal reaches point B before it reaches point A. This causes the returns from point B to be placed on the image closer to the sensor (near range) and obscure point A, as if the top has been overlaid on the foot of the mountain.

LAYOVER

- Mountain top overlain on ground ahead of mountain
- Layover effects *decrease* with increasing look angle
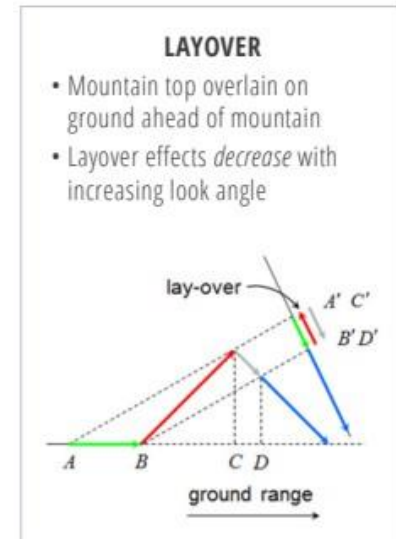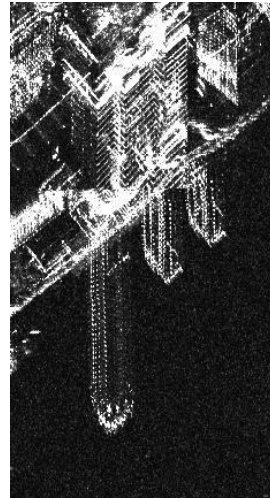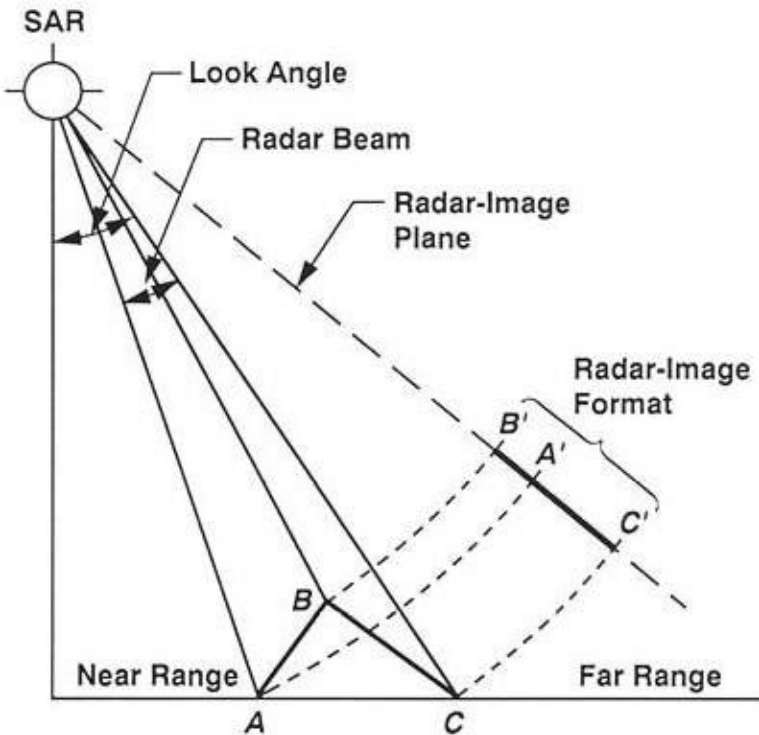
Figure 5. Layover Geometry (Credit: NASA)
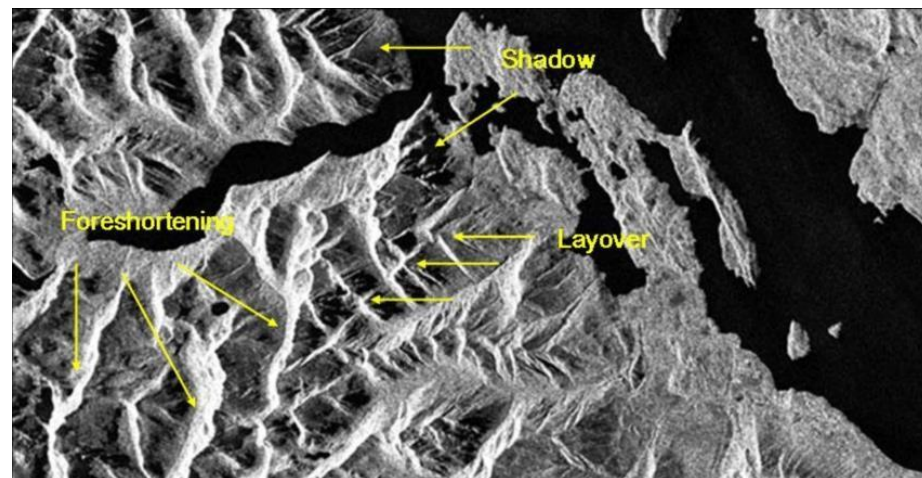
SAR distortions

Chapter 6 (psu.edu)

The wavefront that are equal in distance to the satellite Targets on the same arc (blue dashed line) will end up in the same cell on Radar imagery.
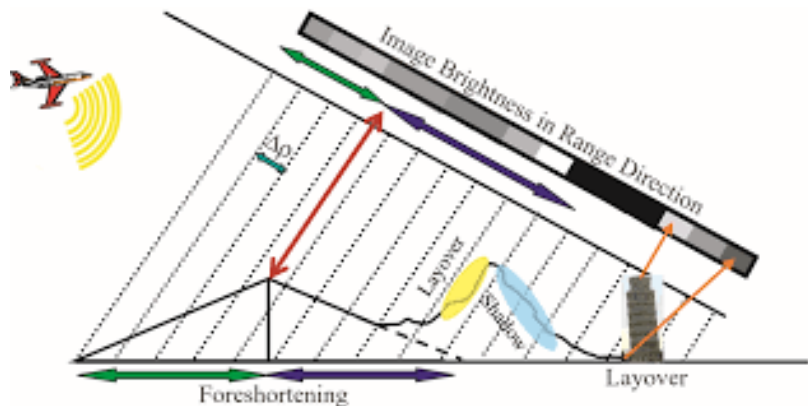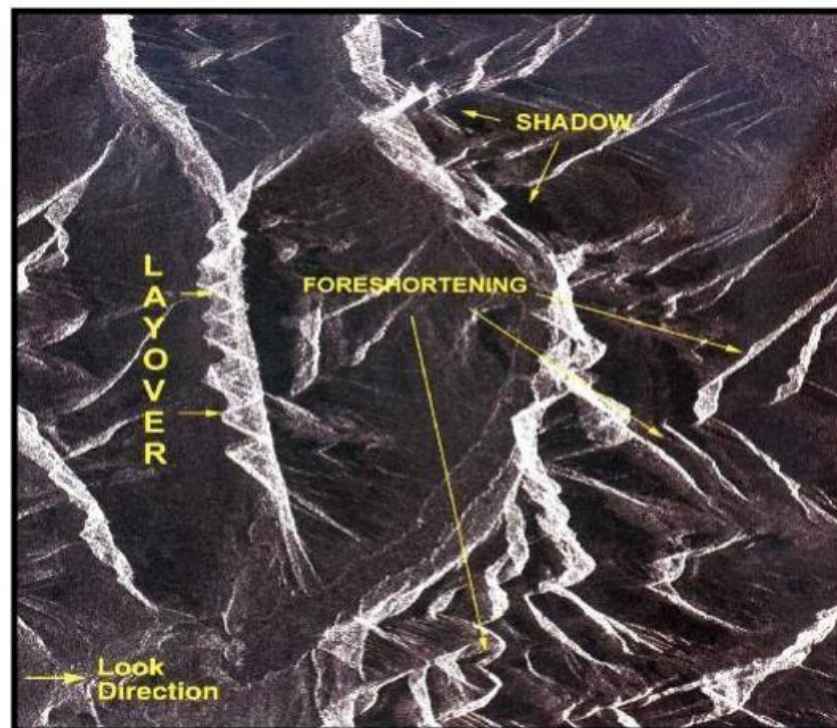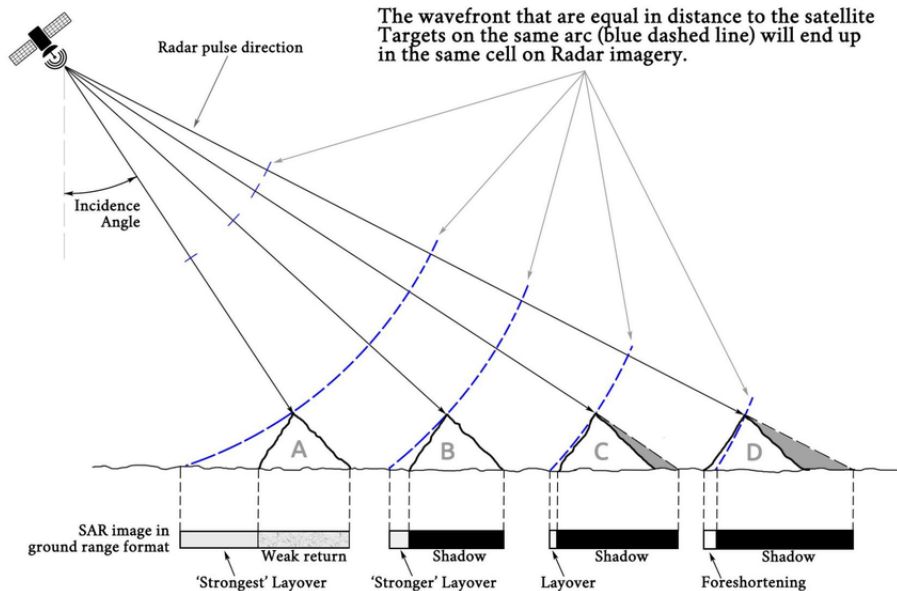
From: RADARSAT Geology Handbook
(RADARSAT International), 1997

Lillesand, T.M.; Kiefer, R.W.; Chipman, J.W. Remote Sensing and Image Interpretation, 7th ed.; John Wiley & Sons, Inc.: Hoboken, NJ, USA, 2015.

Basic measurement

The basic measurement made by a SAR is S (amplitude and phase). This is the complex image.
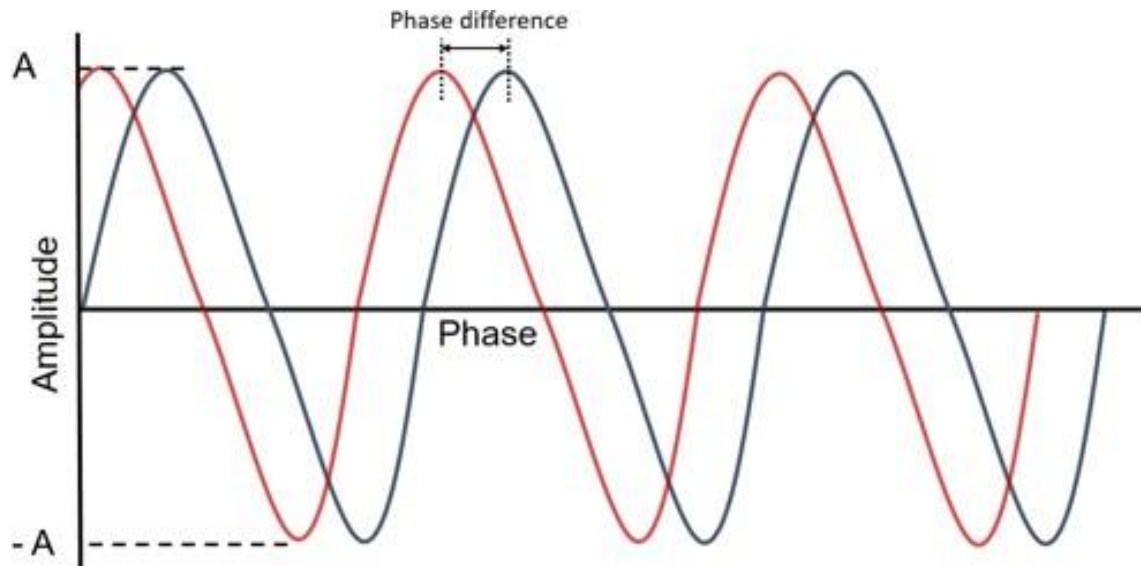
Main types of images:

A is the **amplitude image**.
$I = A^2$ is the **intensity image**.
(the phase of a single image is not exploitable)

Backscatter

- Backscatter is the portion of the outgoing radar signal that the target redirects directly back towards the radar antenna. Backscattering is the process by which backscatter is formed.

- The scattering cross section in the direction toward the radar is called the backscattering cross section.
Sigma nought or Gama nought

- How strong the radar signals reflected back are.
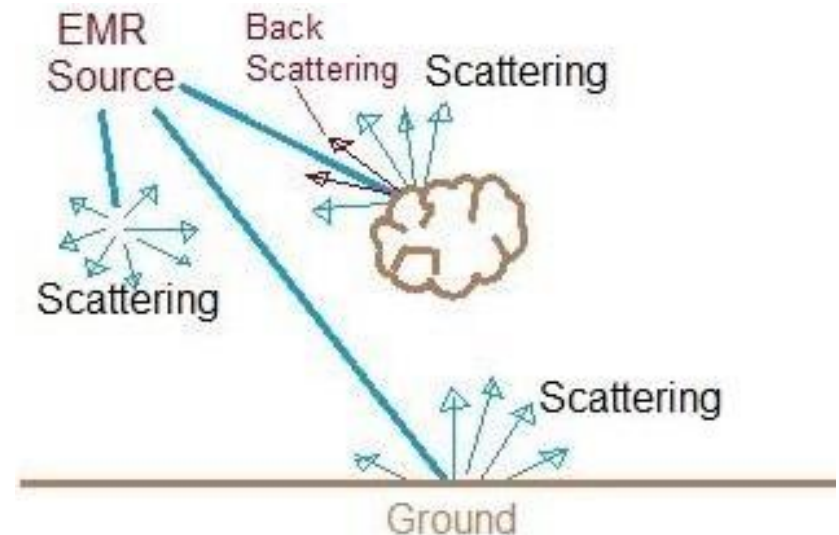
Radar Backscatter

- The radar echo contains information about the Earth's surface, which drives the reflection of the radar signal
- **This reflection is driven by:**
– The frequency or wavelength: radar parameter
– Polarization: radar parameter
– Incidence angle: radar parameter
– Dielectric constant: surface parameter
– Surface roughness relative to the wavelength: surface parameter
– Structure and orientation of objects on the surface: surface parameter

Backscattering Mechanisms
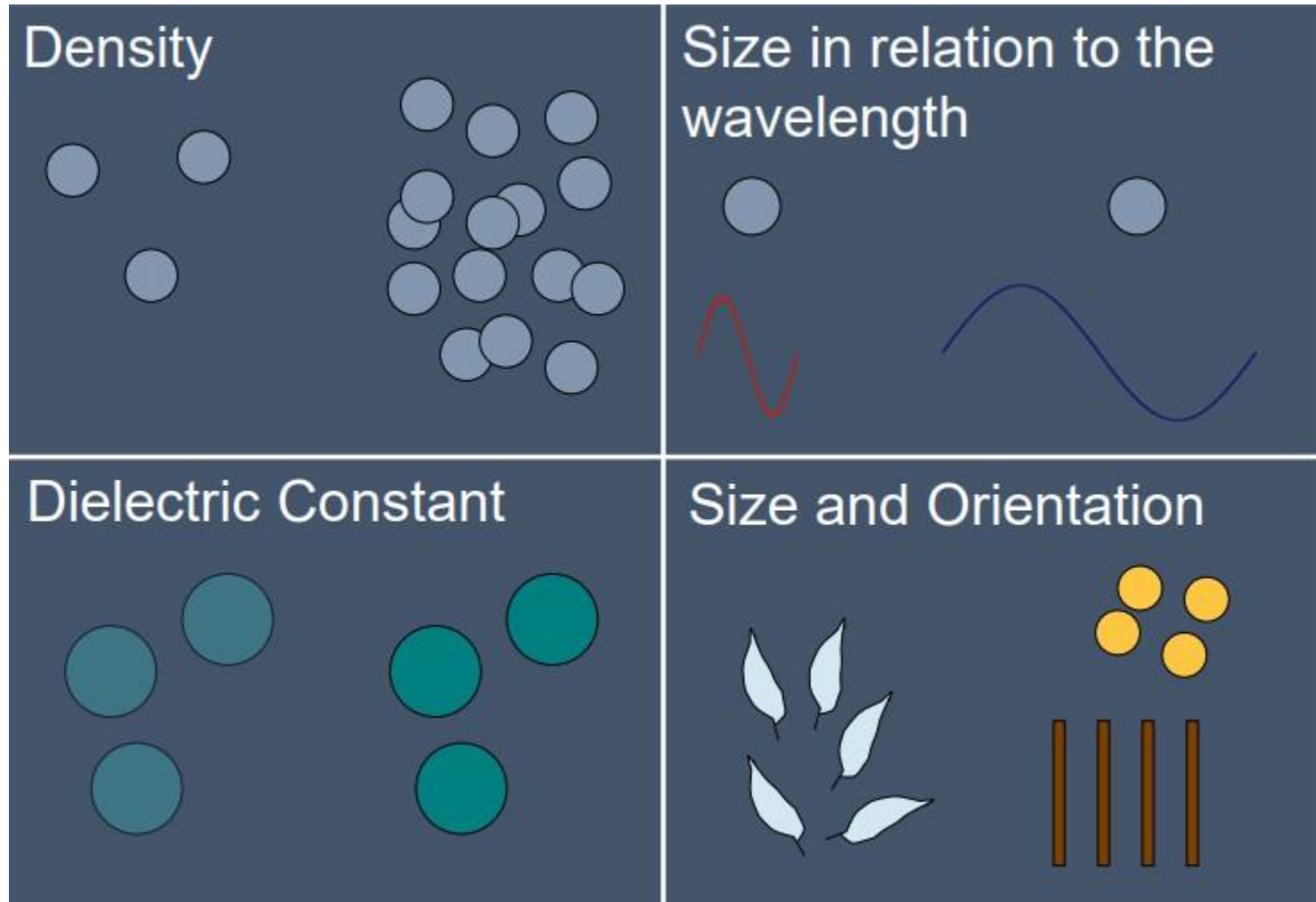
Surface Parameters: Dielectric Constant
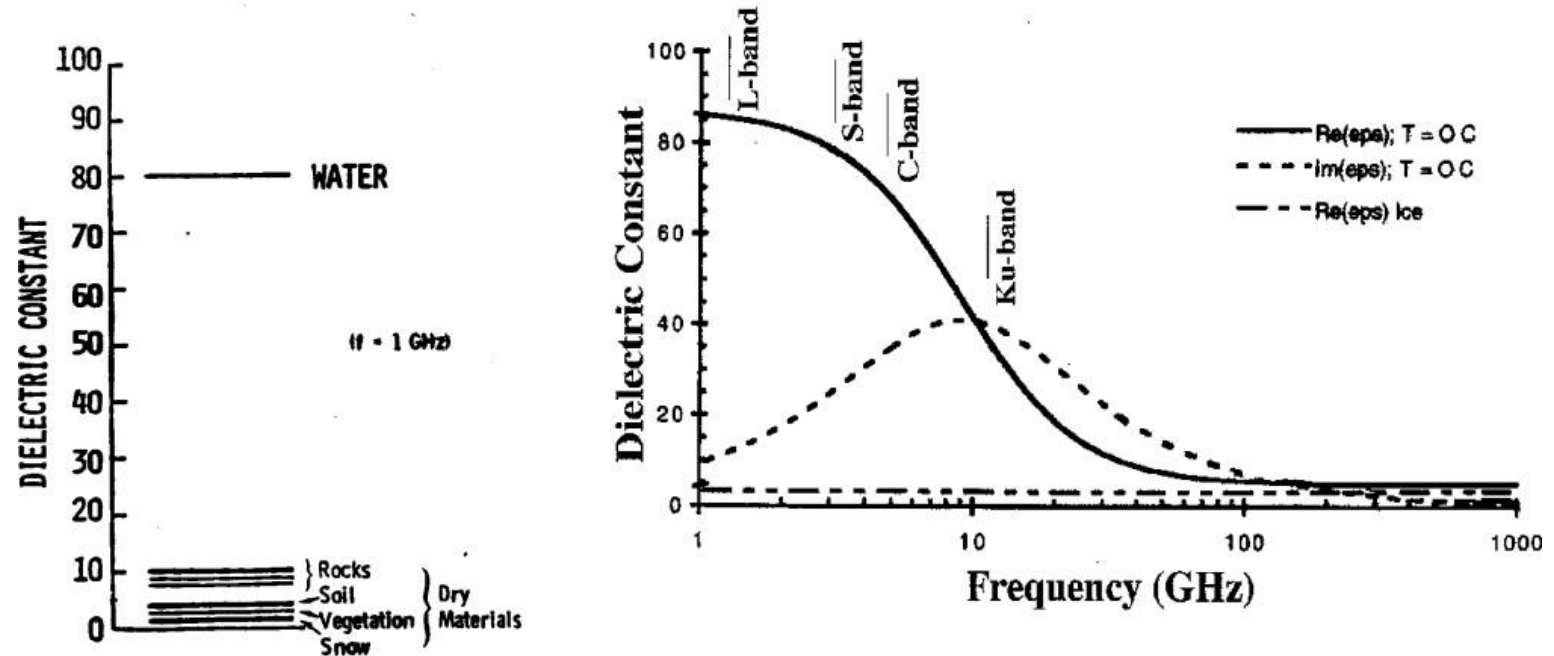
Dielectric Properties of the Surface and its Frozen or Thawed State

- During the land surface freeze/thaw transition there is a change in dielectric properties of the surface
- This causes a notable increase in backscatter
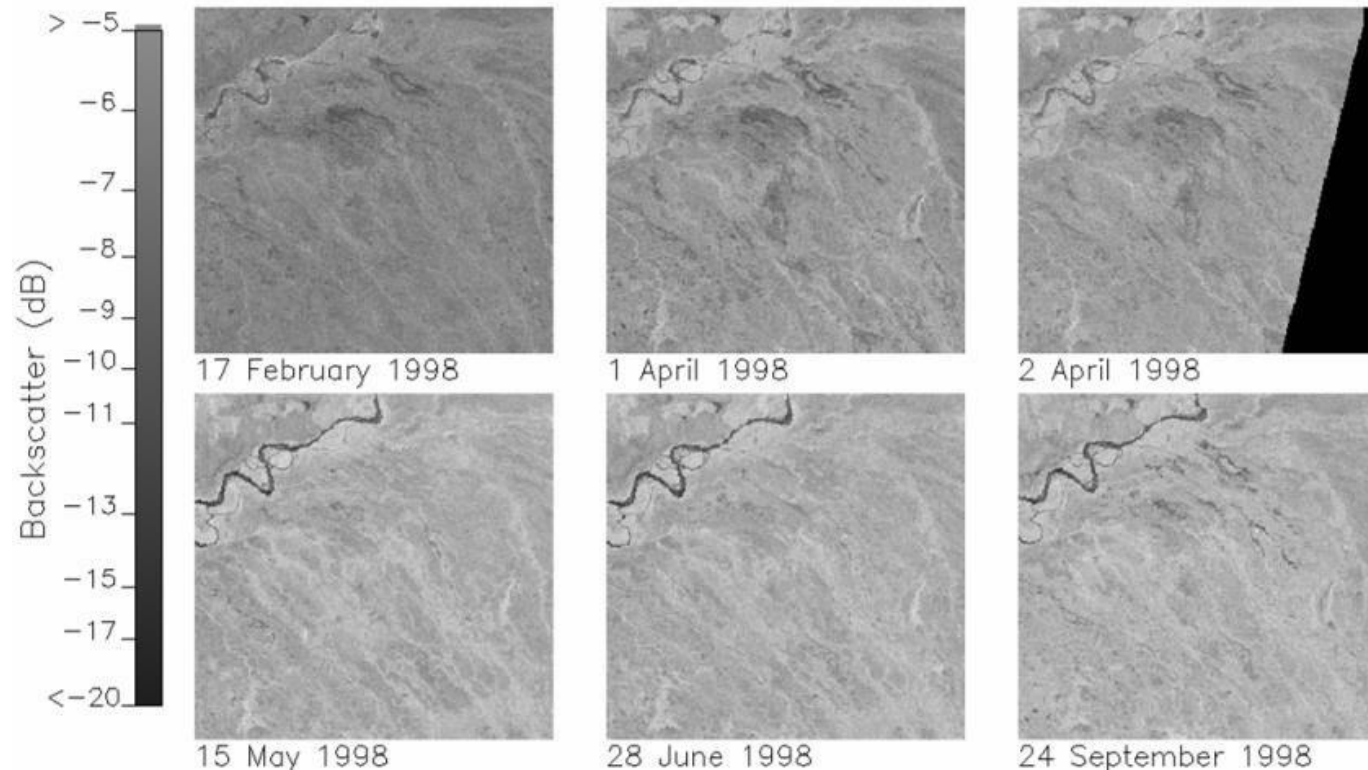
What can SAR data tell you?

- SAR sensors record the interference (Doppler) pattern from echo signals (energy transmitted form the land back to the sensor) over several hundred to several thousand meters along the flight path.

- The received echoes form the raw data matrix or complex image containing amplitude and phase.

- SAR data are also known as 'complex data,' since it comes in multiple parts: the amplitude of the signal (**intensity**) and the signal time delay (**phase**). The intensity and phase parts each tell you something different about the ground.

Surface roughness

- Surface roughness has a large impact on backscatter intensity. The four main types of radar backscatter are specular, diffuse, volume scattering, and double bounce. Each of these backscatter types corresponds to different levels of surface roughness and the resulting intensity value.

Specular

Source: https://storymaps.arcgis.com/stories/fd77b1daf91a4ef99d6f176183e4154a

Surface roughness

Diffuse

Volume scattering

Source: https://storymaps.arcgis.com/stories/fd77b1daf91a4ef99d6f176183e4154a
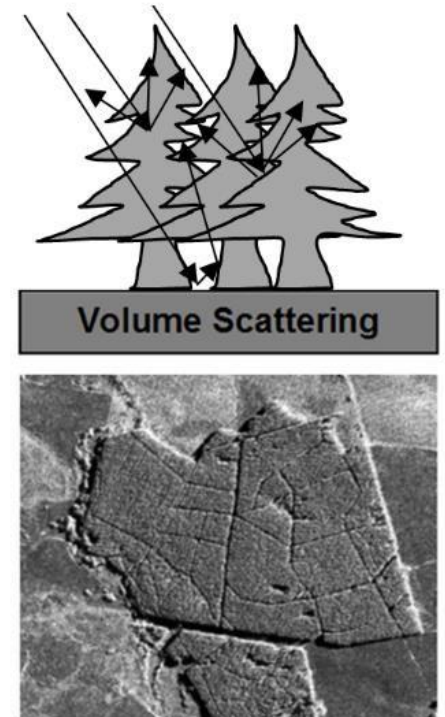
Surface roughness
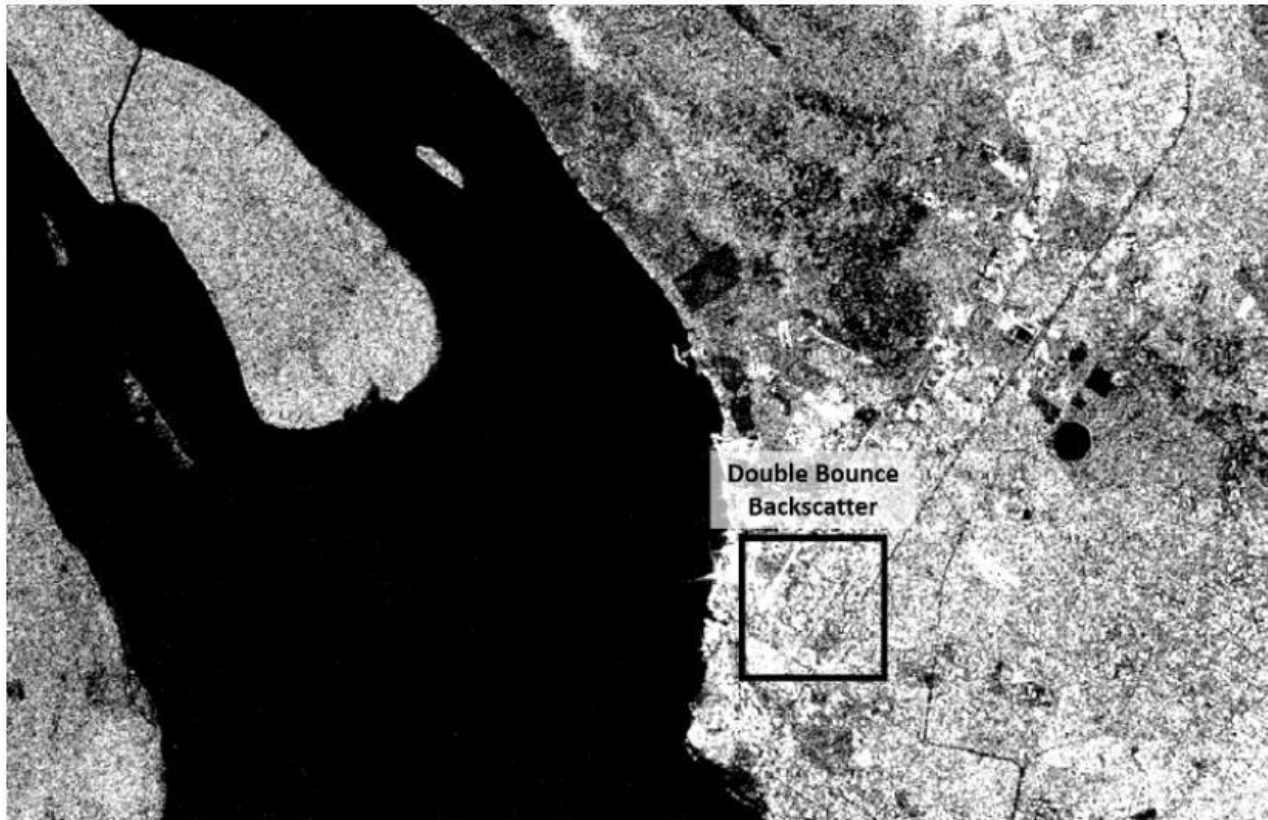
Double bounce

Water content
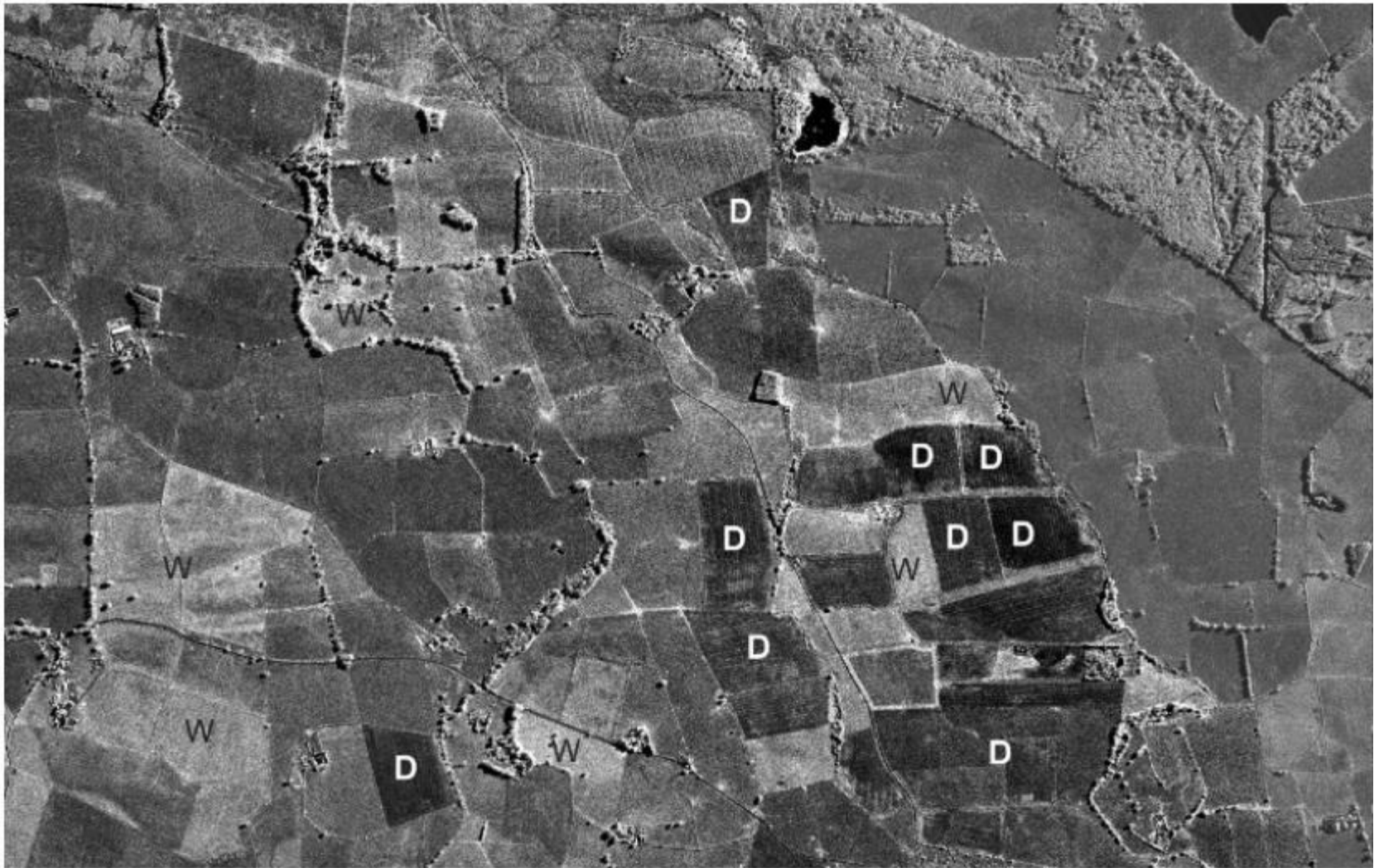
W = Wet Field   D = Dry Field or Bare Soil

Observation: Polarizations

VV   VH

- It is best to get into a habit of exploring the available polarizations when working with SAR data. However, there are a few general guidelines:
- VH and HV (cross-polarized) data is more sensitive to vegetation.
- When doing interferometry, you must use co-polarized (VV or HH) data.

Radar Signal Interaction

- The radar signal is primarily sensitive to surface structure
- The scale of surface relative to the wavelength determine how rough or smooth they appear and how bright or dark they will appear on the image
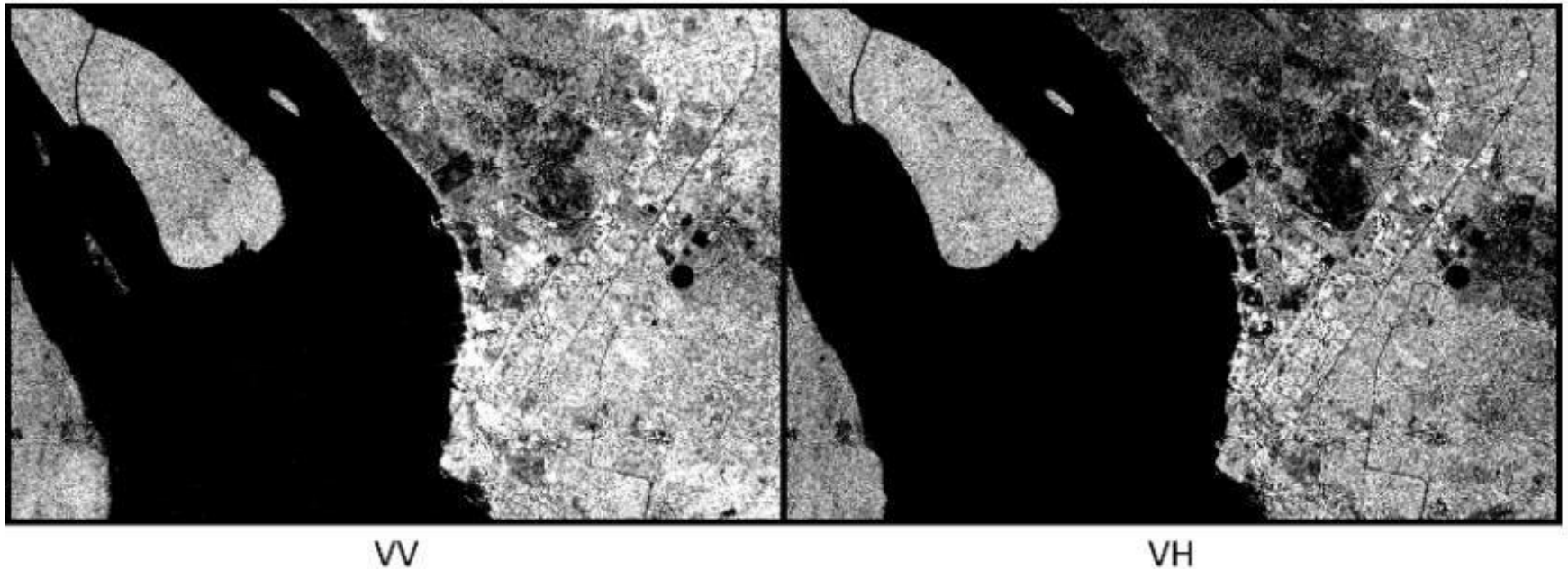
Backscattering Mechanisms

Smooth Surface

Rough Surface

Backscattering Mechanisms

Double-bounce

Vegetation Layer

Source: Erika Podest, Basics of SAR: NASA-ARSET Applied Remote Sensing Training

Surface Roughness

Smooth: no return
$<< \lambda$

Slightly Rough: slightly diffuse
$< \lambda$

Moderately Rough: moderately diffuse
$> \lambda$

Very Rough: very diffuse
$>> \lambda$
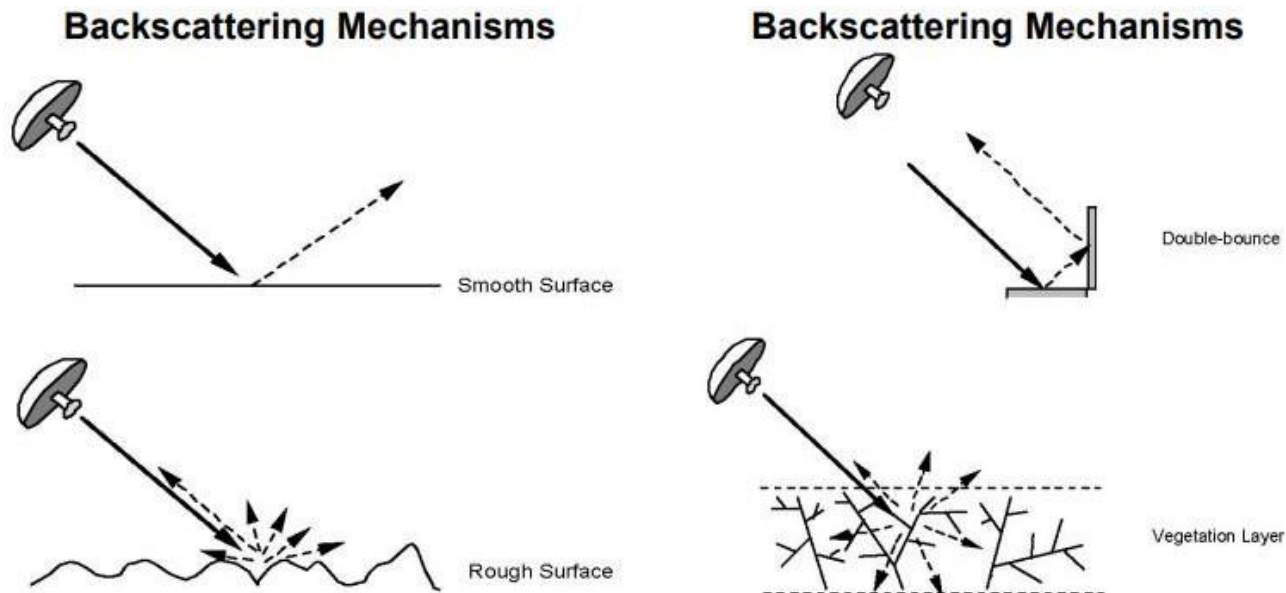
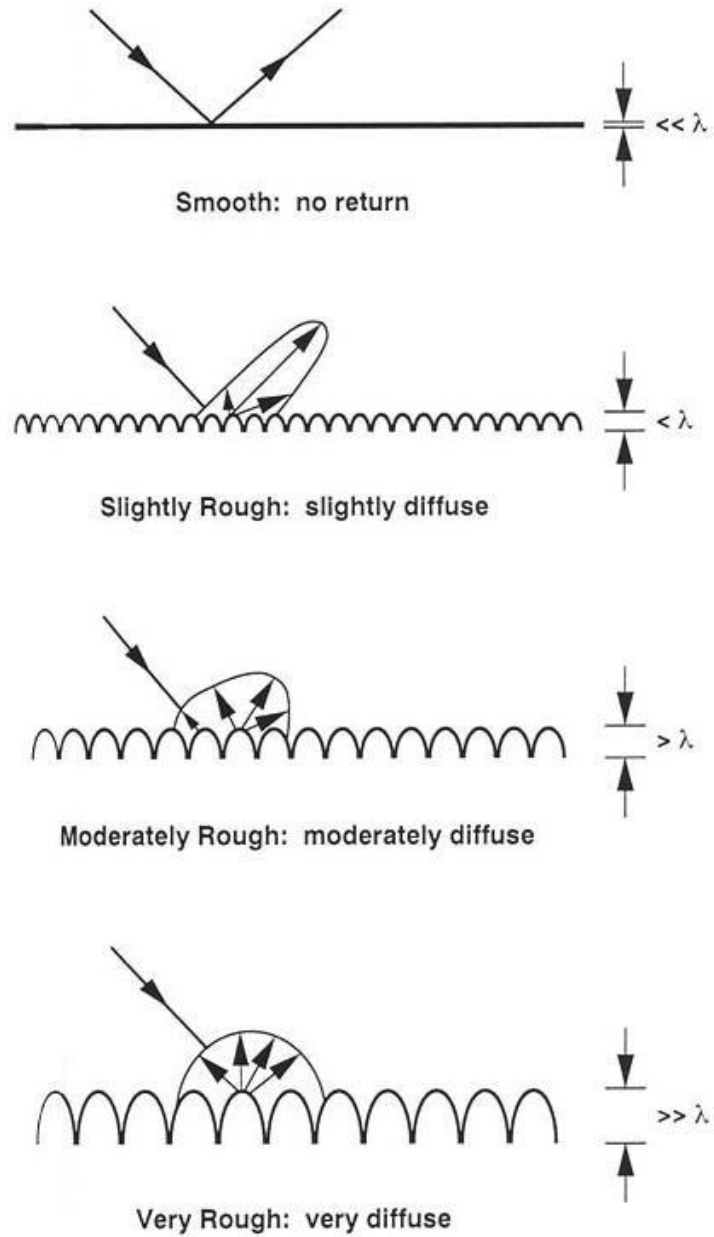Figure 9. Surface Roughness Scattering (Credit: NASA)

SAR signal penetration by sensor wavelength λ
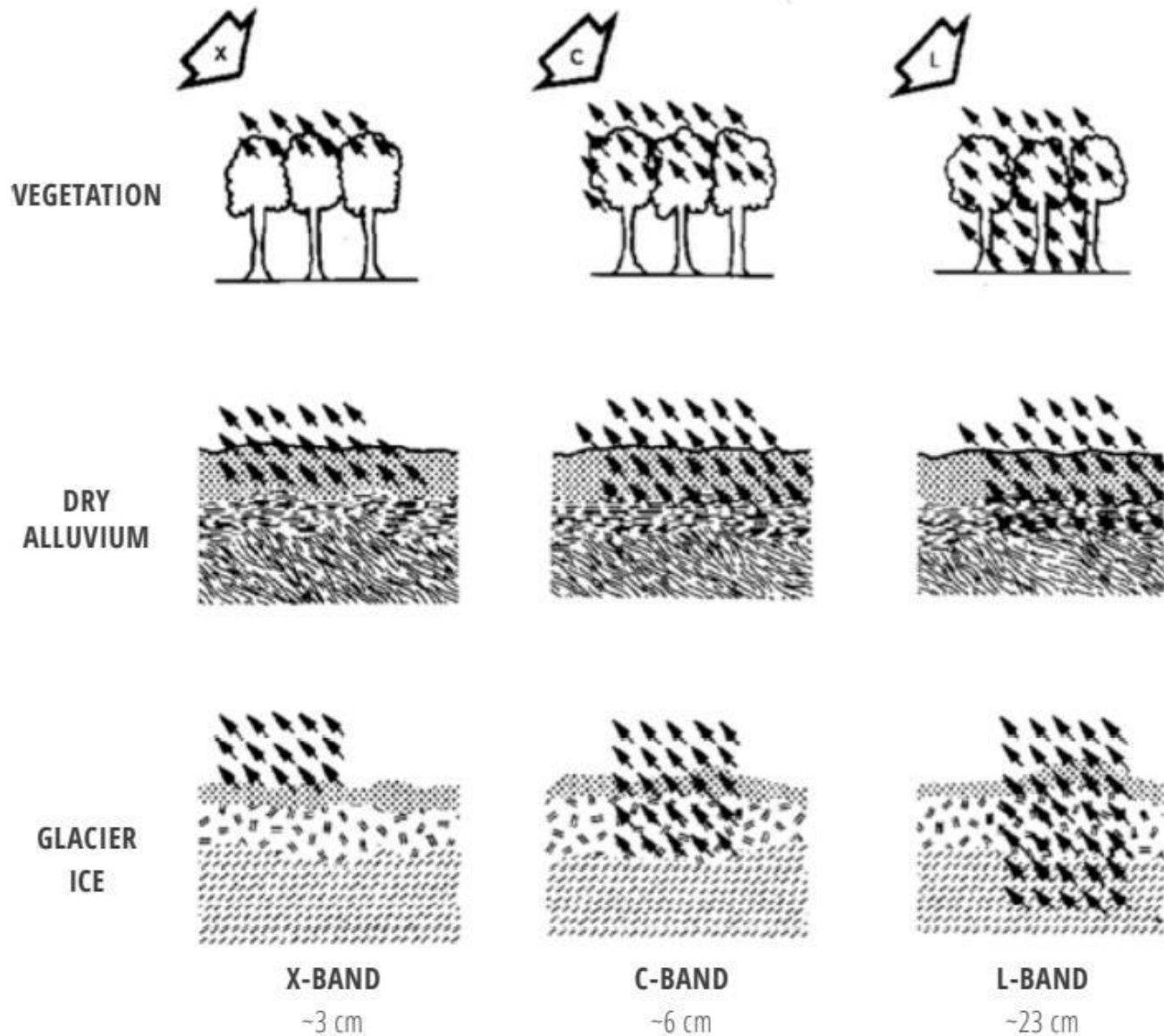
Source: Introduction to SAR - HyP3 (alaska.edu)

Radar Backscatter in Forests
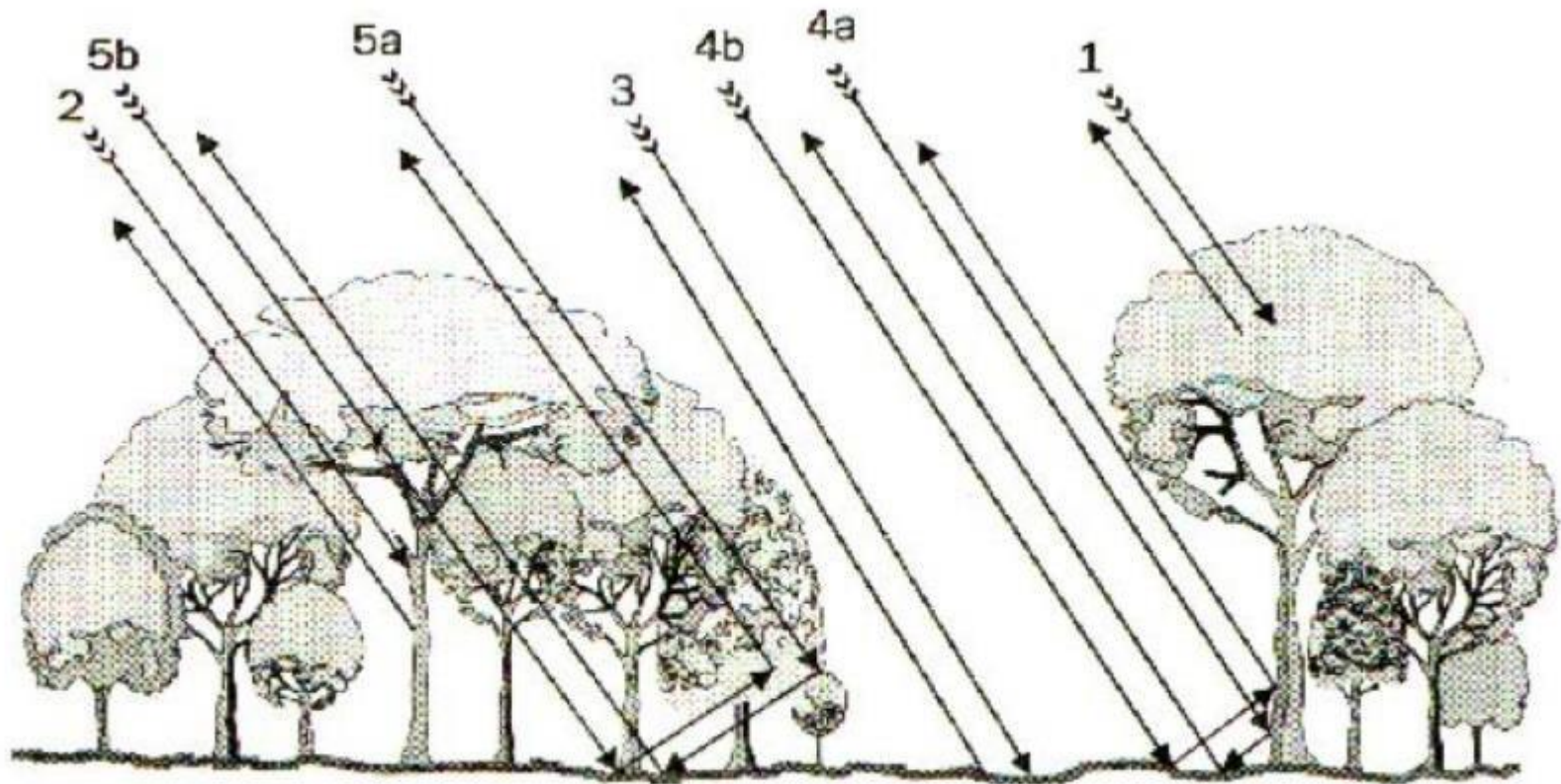
Dominant backscattering sources in forests: (1) crown volume scattering, (2) direct scattering from tree trunks, (3) direct scattering from the soil surface, (4a) trunk - ground scattering, (4b) ground - trunk scattering, (5a) crown - ground scattering, (5b) ground - crown scattering.

Scatterers contribution

Leaves, Needles

Primary Branches

Secondary branches

Higher order branches

Trunk
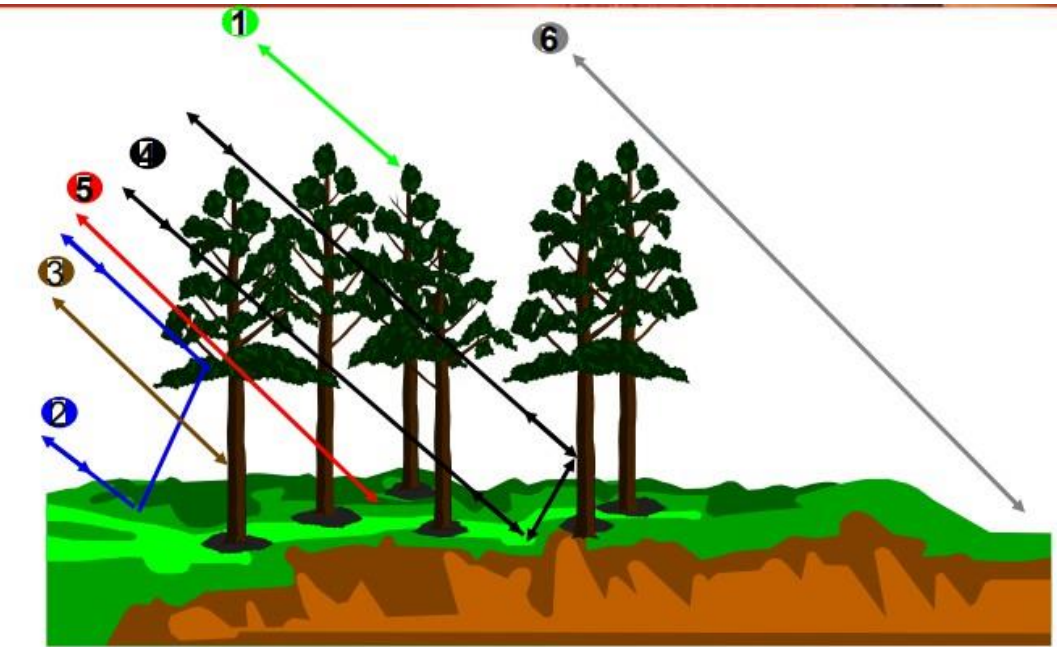
1) Direct Crown scattering
2) Direct trunk-ground
3) Trunk scattering

4) Multiple trunk-ground
5) Attenuated ground
6) Direct ground scattering

14/02/2024

Scattering mechanisms

Source: Thuy Le Toan, Introduction to SAR: ESA Advanced course in land remote sensing (2010)
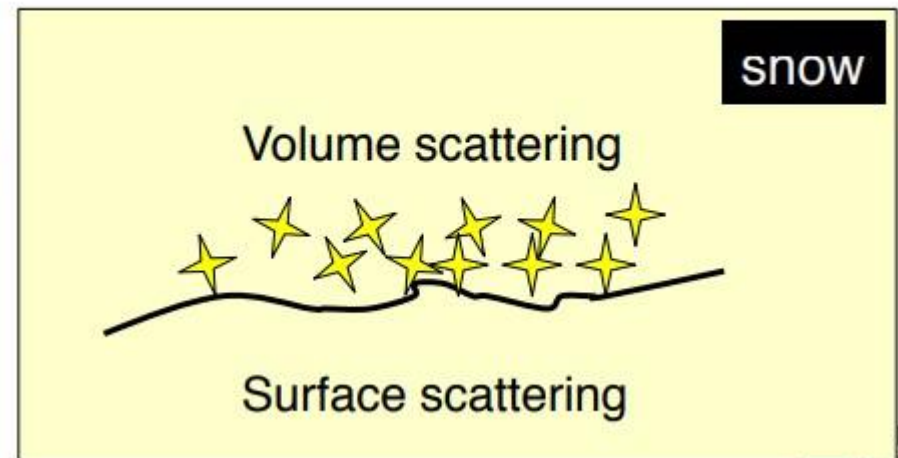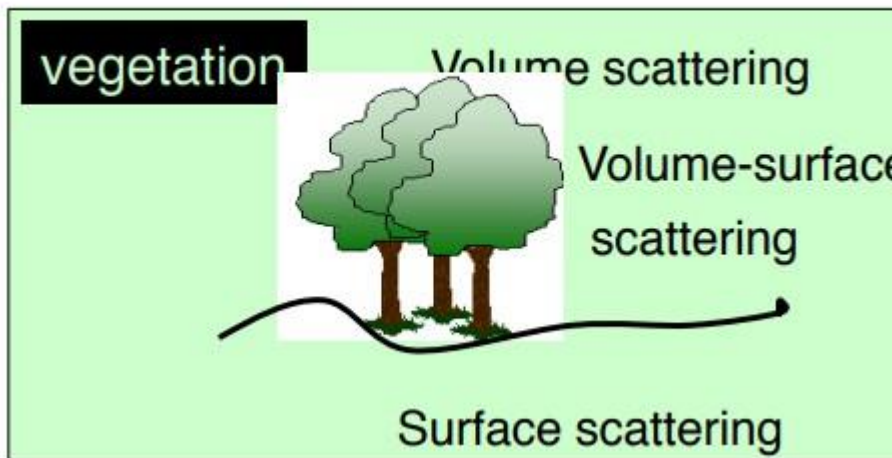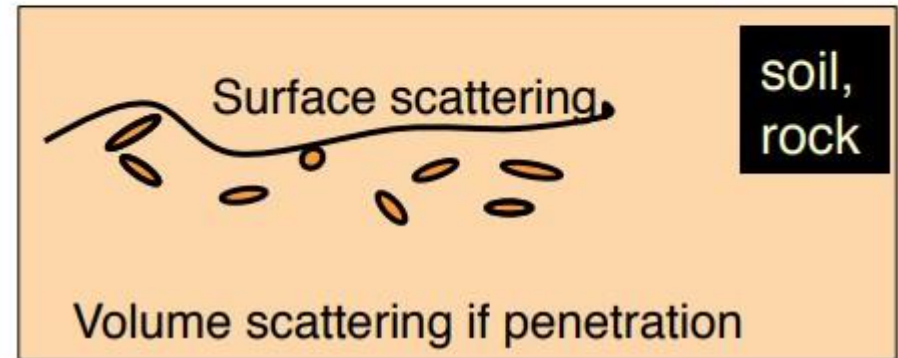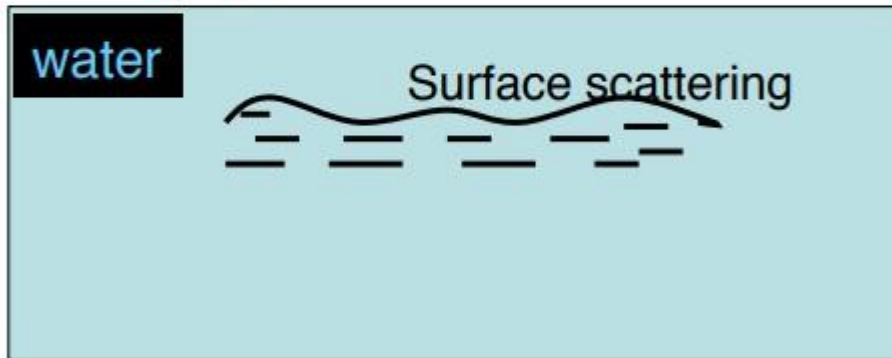
What are the scatterers in the volume scattering?

Austrian pine	X band $\lambda = 3$ cm	L band $\lambda = 27$ cm	P band $\lambda = 70$ cm	VHF $\lambda > 3$ m
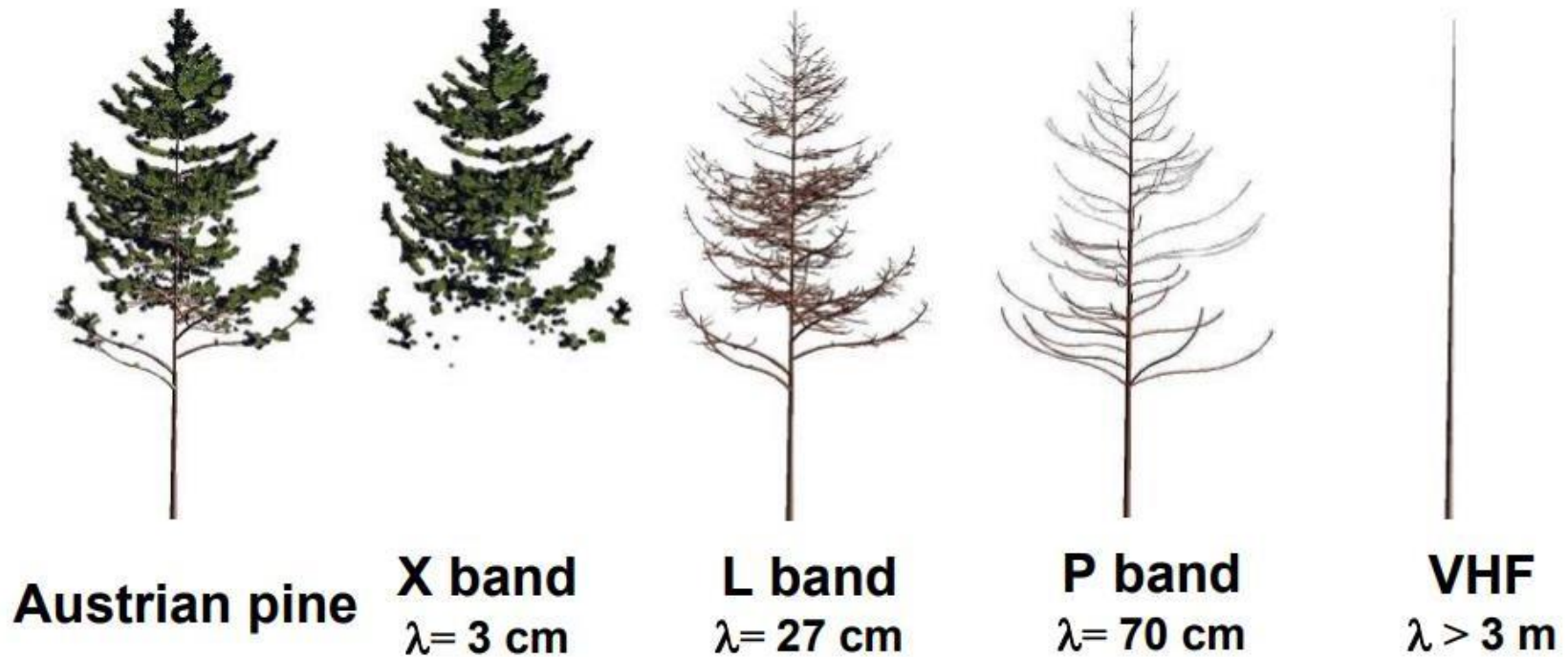
The main scatterers in a canopy are the elements having dimension of the order of the wavelength
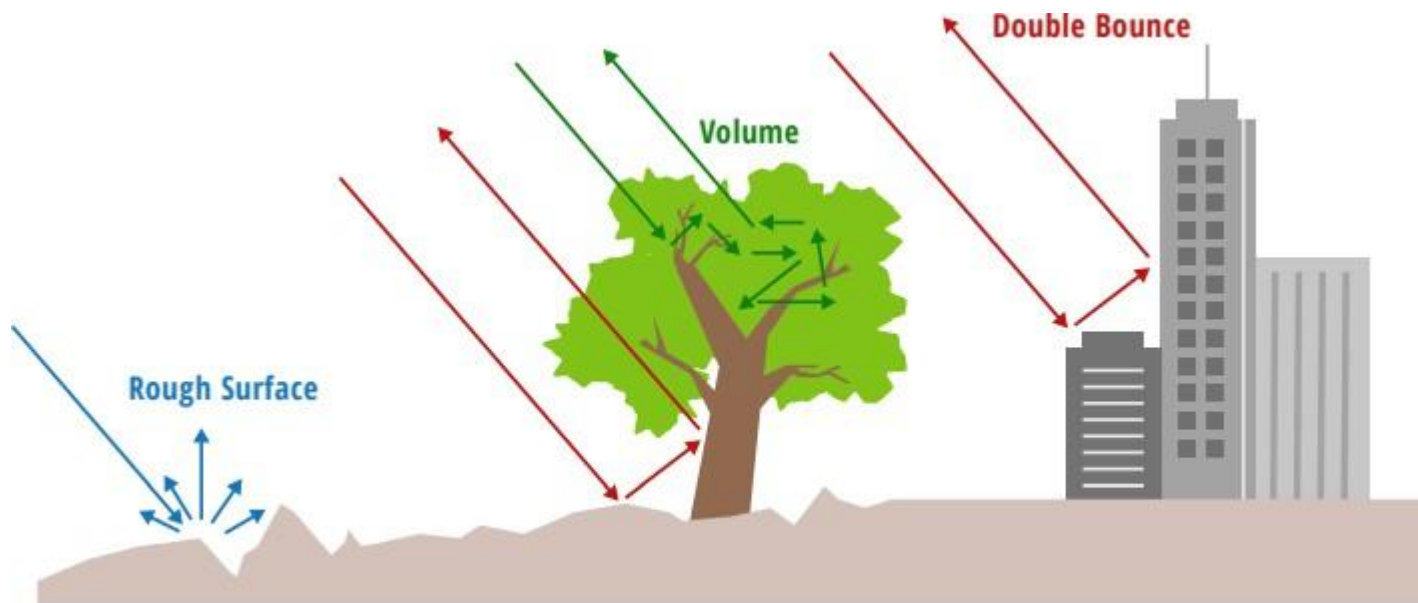
Schematic sketch of the three main scattering types considered for SAR data.

RELATIVE SCATTERING STRENGTH BY POLARIZATION:

Rough Surface Scattering	$\lvert S_{W} \rvert > \lvert S_{HH} \rvert > \lvert S_{HV} \rvert$ or $\lvert S_{VH} \rvert$
Double Bounce Scattering	$\lvert S_{HH} \rvert > \lvert S_{W} \rvert > \lvert S_{HV} \rvert$ or $\lvert S_{VH} \rvert$
Volume Scattering	Main source of $\lvert S_{HV} \rvert$ and $\lvert S_{VH} \rvert$

Relative scattering strength by polarization

[NASA ARSET: Basics of Synthetic Aperture Radar (SAR), Session 1/4 – YouTube](#) (min 33:49 -38:23)

SAR signal penetration by sensor wavelength λ

Basics of Polarimetry
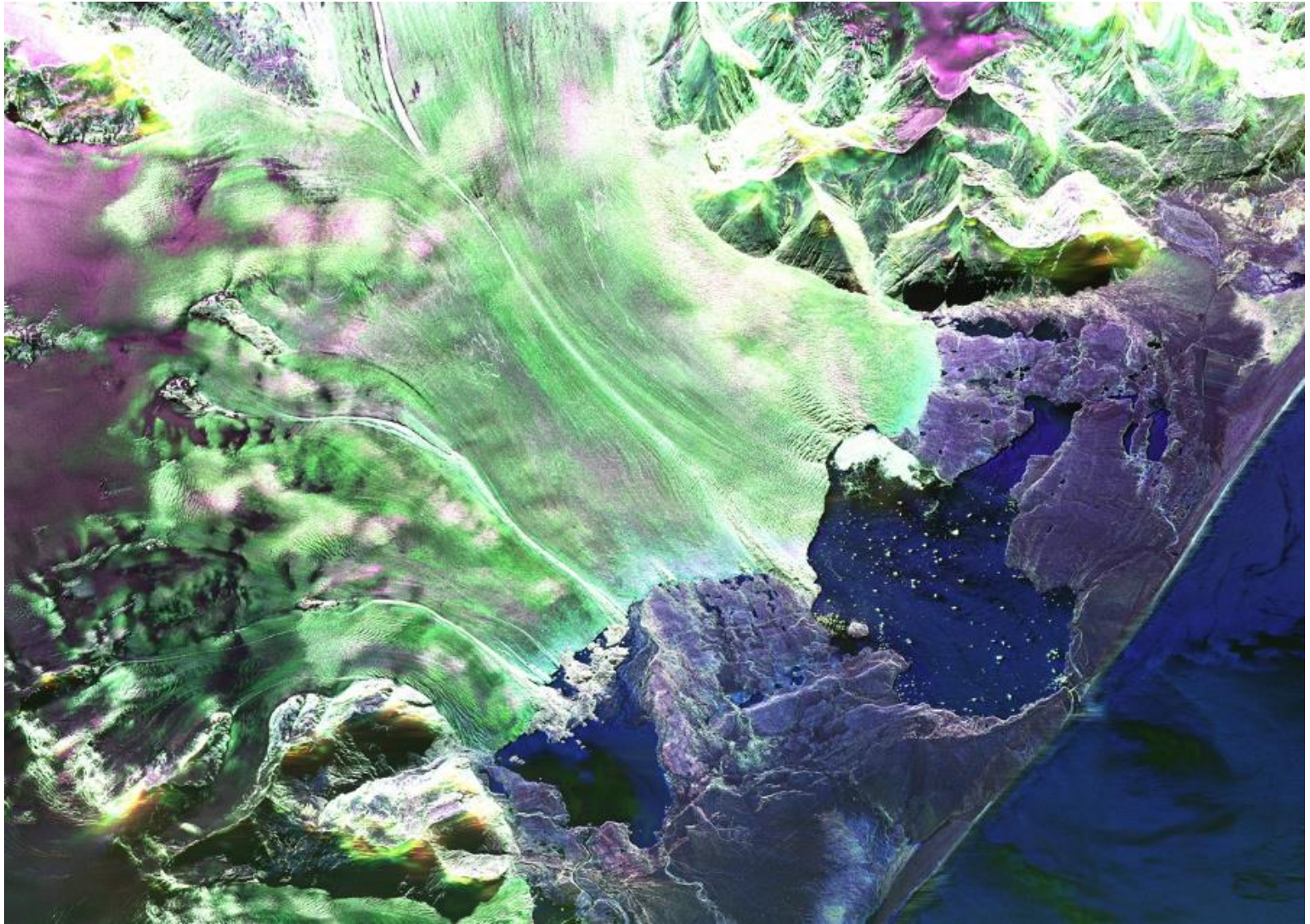
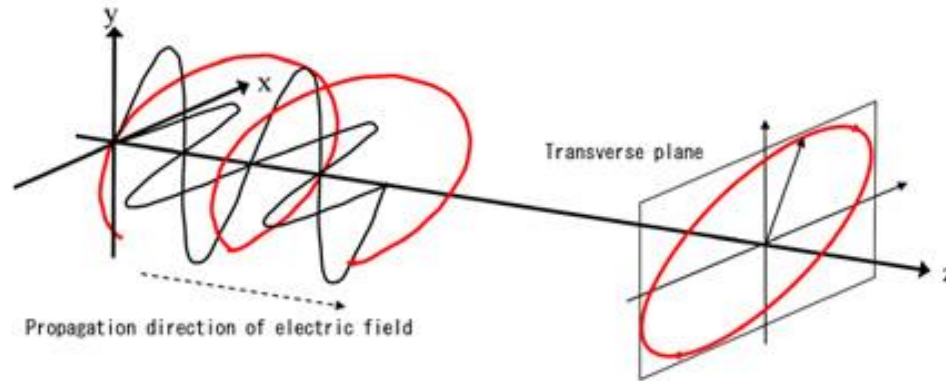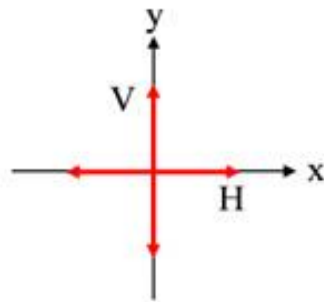# Polarization

Polarization refers to the direction of travel of an electromagnetic wave vector's tip: vertical (up and down), horizontal (left to right), or circular (rotating in a constant plane left or right). The direction of polarization is defined by the orientation of the wave's electric field, which is always 90°, or perpendicular, to its magnetic field.

Propagation direction of electric field

(i)   Locus of an elliptically polarized wave

(a) Horizontal polarization,
Vertical polarization
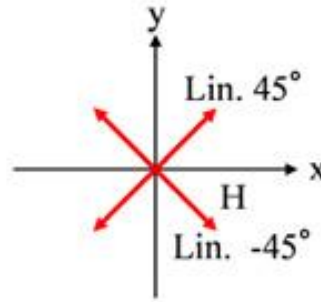
(b) Linear 45 degree polarization,
Linear -45 degree polarization,
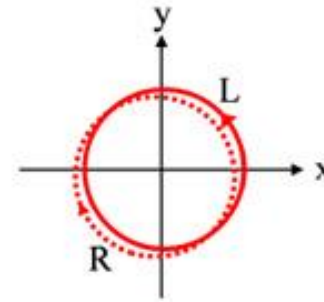
(c) Left circular polarization,
Right circular polarization

(ii)   Typical polarizations

(a) HH

(b) HV and VH

(c) VV

(iii)   Scattering with respect to polarization

Source: https://www.eorc.jaxa.jp/ALOS/en/img_up/pal_polarization.htm

Source: https://nisar.jpl.nasa.gov/mission/get-to-know-sar/polarimetry/
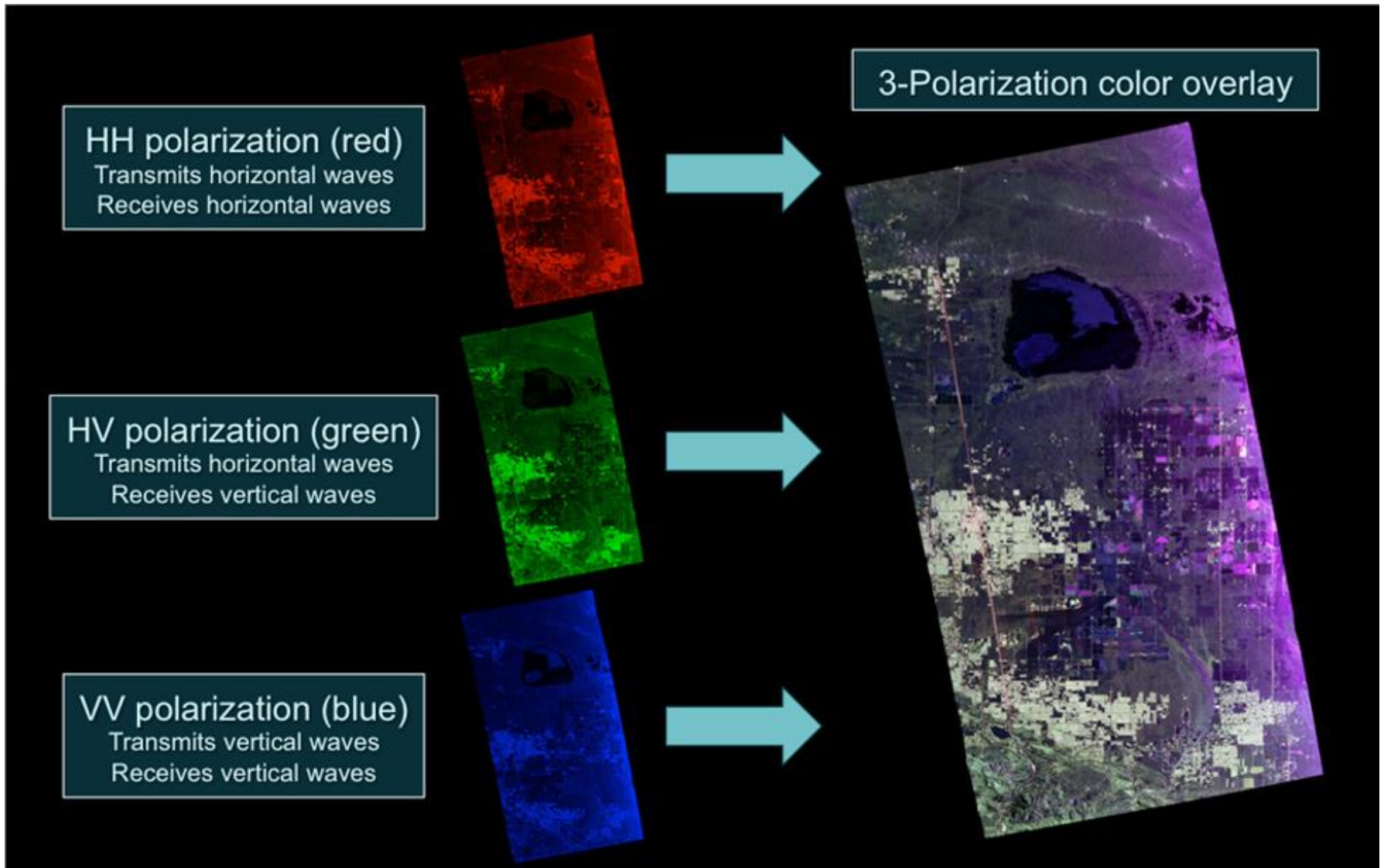
Polarization

HH   HV   VV   HH, HV, VV
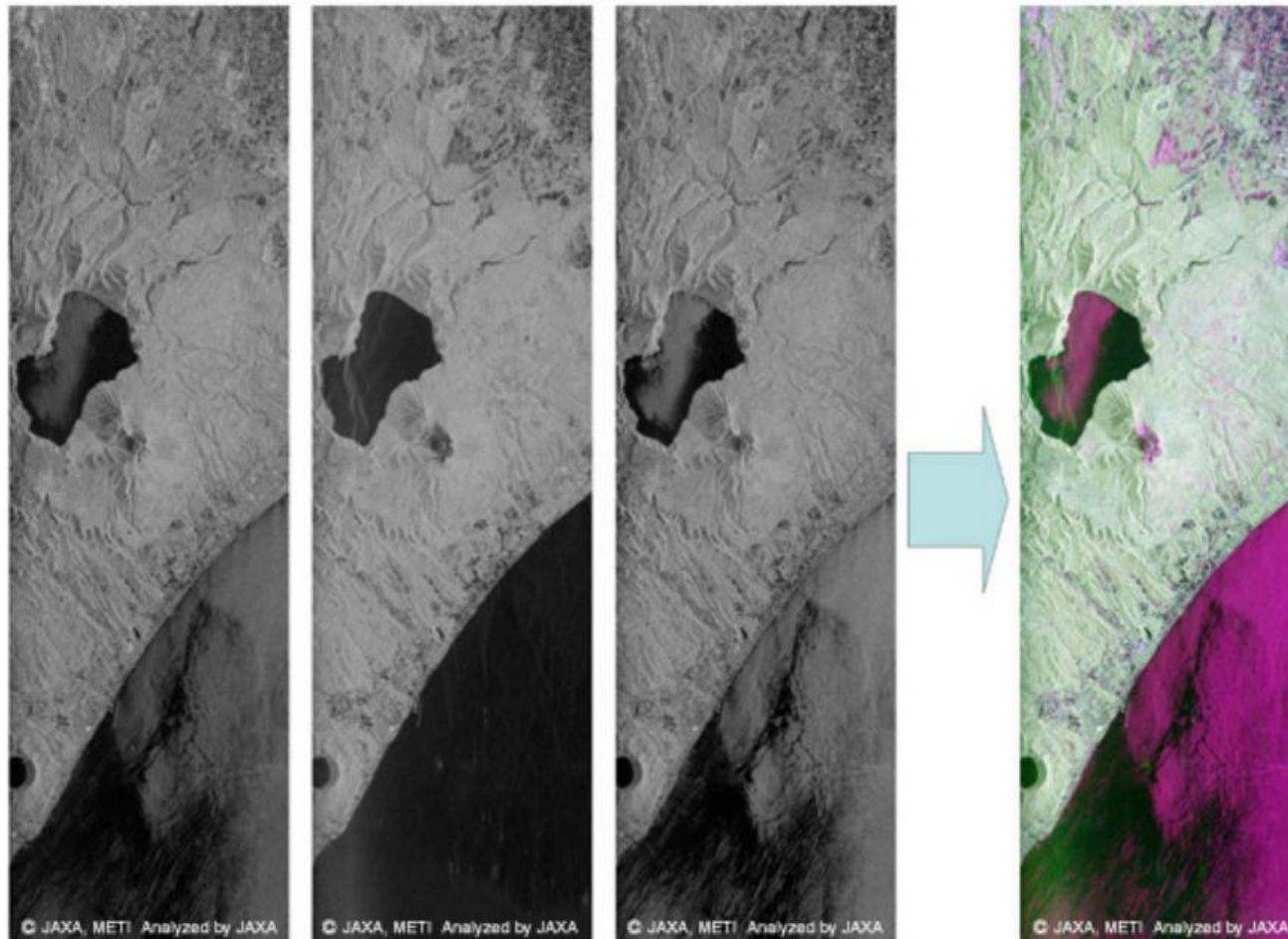
2006/08/19 01:17(UT) ALOS/PALSAR POLARIMETRY

Source: https://www.eorc.jaxa.jp/ALOS/en/img_up/pal_polarization.htm

SAR Applied to Forest Studies

https://climate.nasa.gov/images-of-change?id=727#727-deforestation-in-argentinas-gran-chaco

Droughts

GLOBAL CLIMATE CHANGE
Vital Signs of the Planet | Images of Change

Before

After

BEFORE AND AFTER

Drought in Lake Powell, Arizona and Utah

March 25, 1999 - May 13, 2014

CURTAIN TOGGLE 2 - UP

https://climate.nasa.gov/images-of-change?id=526#526-drought-in-lake-powell-arizona-and-utah

Floods

https://climate.nasa.gov/images-of-change?id=659#659-flooding-in-kerala-india

40

Example of SAR applications
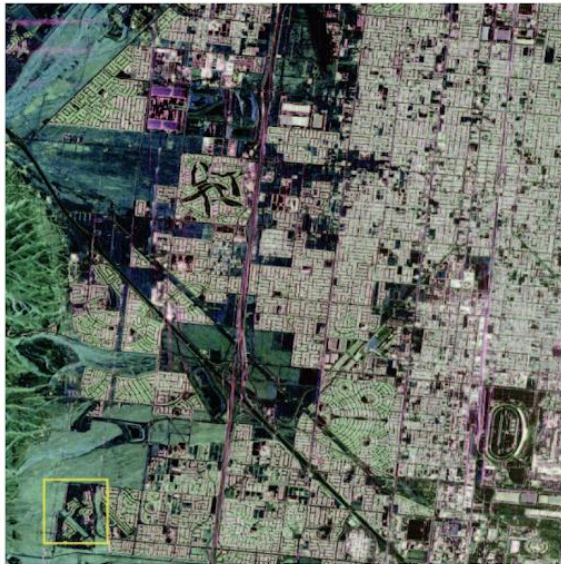
(a)   (b)   (c)

■ Urban Change (UC)   ■ Natural Unchanged (NU)   ■ Urban Unchanged (UU)

The global forest above-ground biomass pool for 2010 estimated from high-resolution satellite observations

- The terrestrial forest carbon pool is poorly quantified, in particular in regions with low forest inventory capacity.

- By combining multiple satellite observations of synthetic aperture radar (SAR) backscatter around the year 2010, we generated a global, spatially explicit dataset of above-ground live biomass (AGB; dry mass) stored in forests with a spatial resolution of 1 ha.

- Using an extensive database of 110 897 AGB measurements from field inventory plots, we show that the spatial patterns and magnitude of AGB are well captured in our map with the exception of regional uncertainties in high-carbon-stock forests with AGB > 250 Mg ha−1, where the retrieval was effectively based on a single radar observation.

- Uncertainty of estimated AGB was about 50-60% of the mean AGB reference
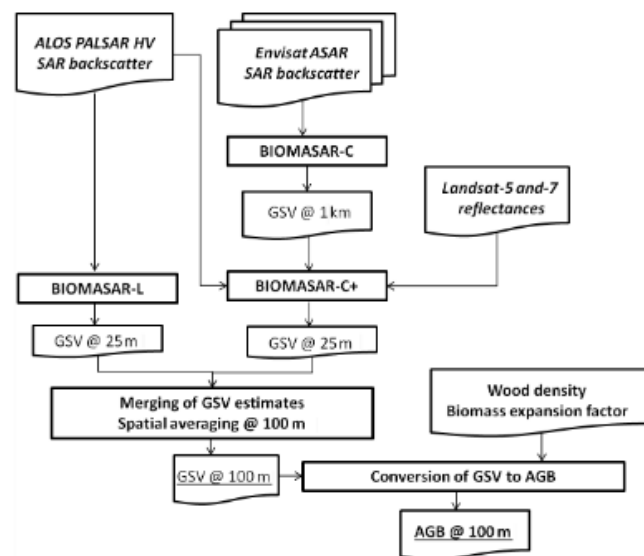
Figure 1. Flowchart of the AGB retrieval approach.

GSV- growing stock volume
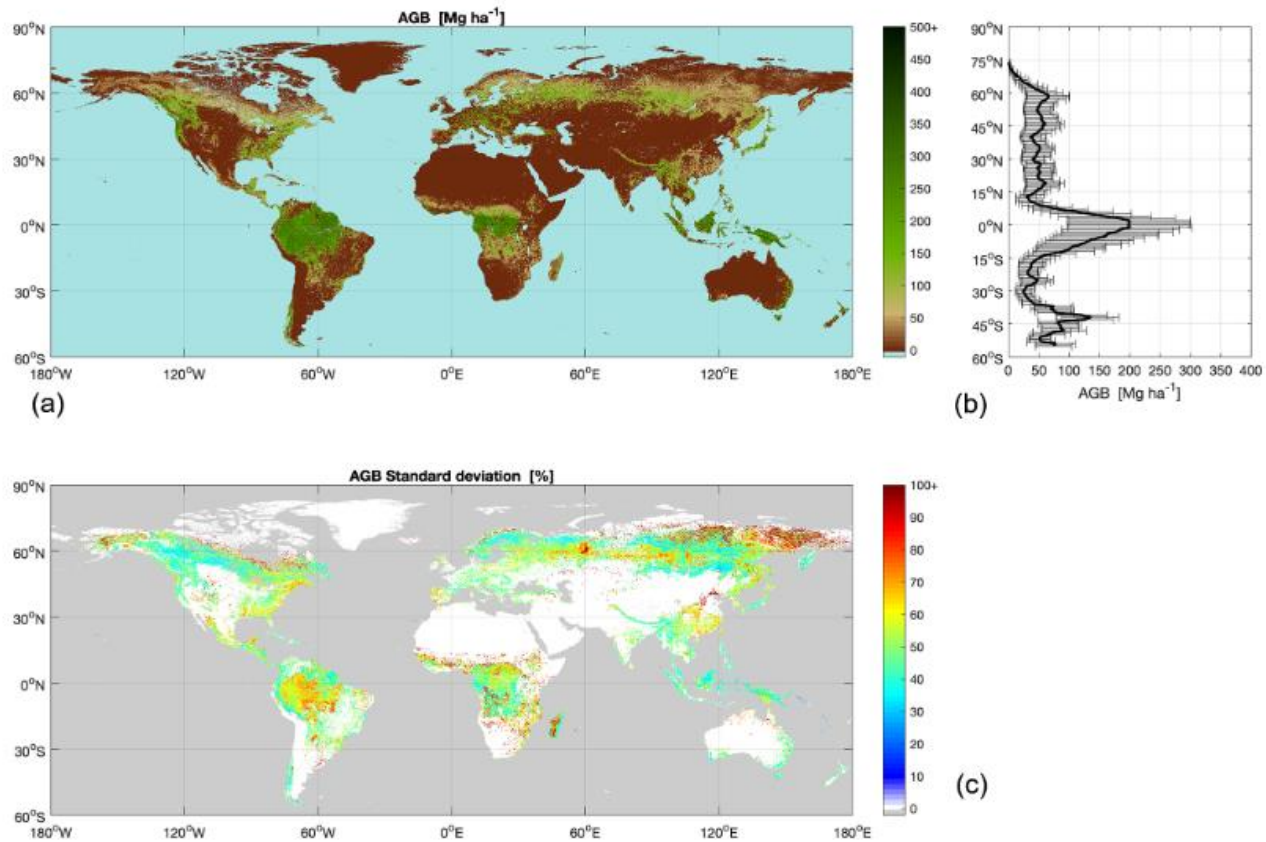
Figure 2. Map estimates of AGB (**a**) and AGB standard deviation expressed relative to the AGB (**b**). The colour bar of the AGB map has been truncated at 500 Mg ha^{-1} to increase contrast. Similarly, the colour bar of the AGB relative standard deviation has been truncated at 100 %. The right-hand panel shows the profile of average AGB along latitude (thick solid line) and the two-sided average standard deviation of AGB at a given latitude (horizontal bars).
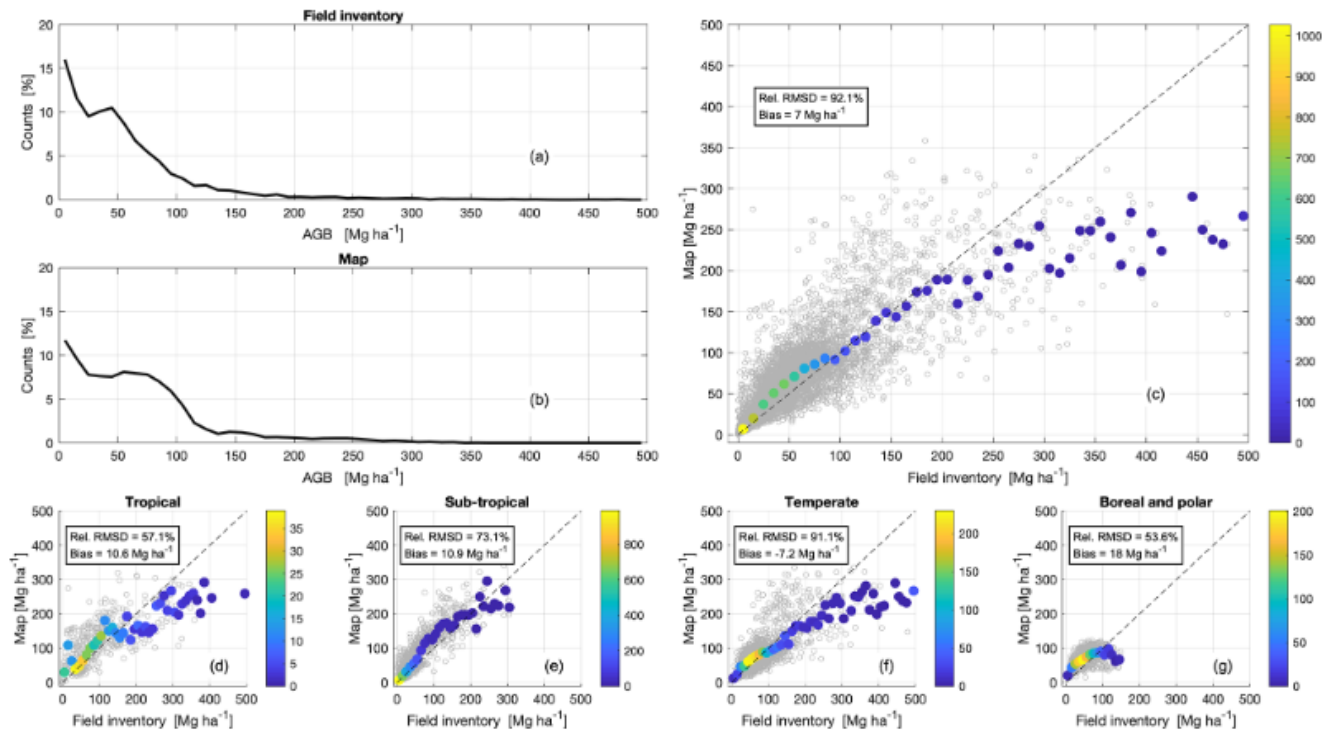
Figure 5. Histograms of AGB from the field inventory database (**a**) and the map (**b**) for 0.1° grid cell values. (**c**) Scatterplot of map AGB against field inventory values for 0.1° grid cells (grey circles); the filled circles show the median AGB of the map values in each 10 Mg ha^{-1} wide interval of field inventory AGB values. The colour bar represents the number of grid cells within a given AGB interval. Similar scatterplots are given for the tropical zone (**d**), the subtropical zone (**e**), the temperate zone (**f**), and the boreal and polar zones (**g**) according to the FAO global ecological zones. On each scatterplot, we report the root mean square difference (RMSD) between map and field inventory AGB relative to the mean value of the reference AGB and the bias, i.e. the difference between mean values of the map AGB and the reference AGB. To improve presentation and because of the paucity of grid cells with AGB above 500 Mg ha^{-1}, axes are truncated at 500 Mg ha^{-1}.

Aboveground biomass and multisensory approach
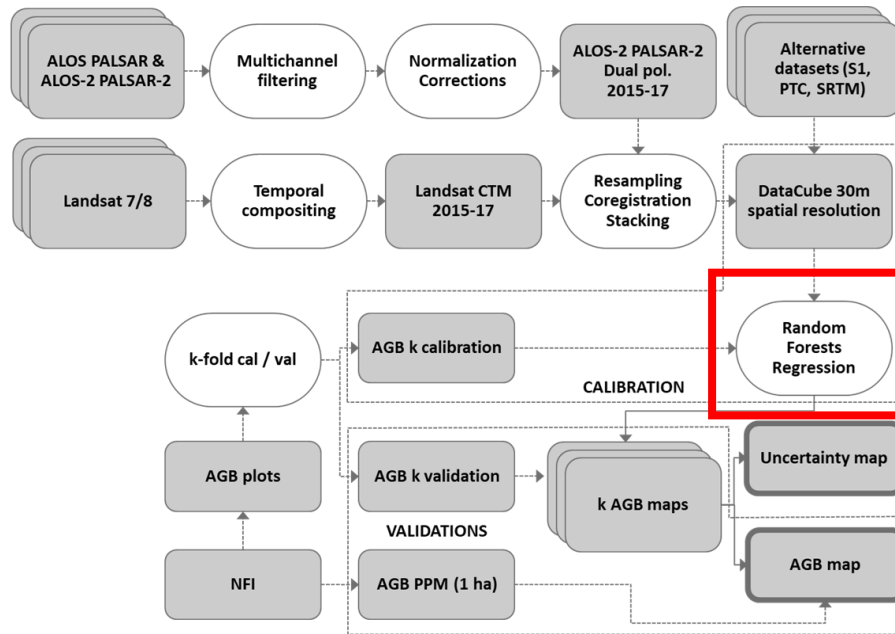
AGB Colombian Amazon
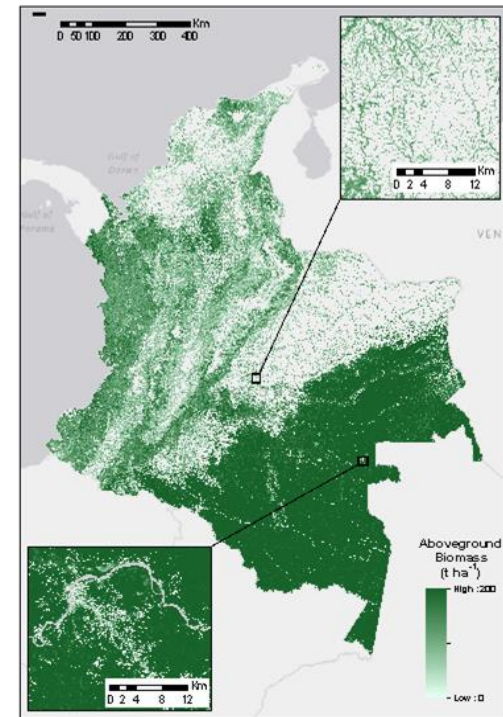
Terabytes of data for National coverage!

Woody aboveground biomass mapping of the Brazilian savanna (Cerrado) with a multi-sensor and machine learning approach

The Brazilian Savanna, known as Cerrado (*Cerrado sensu lato* (s.l.))*, is the second largest biome in South America.

Bispo, et al. 2020, Remote Sensing https://doi.org/10.3390/rs12172685

- The Cerrado Biome comprises different physiognomies due to variations of soil, topography and human impacts.
- The gradients of tree density, tree height, above ground biomass (AGB) and wood species cover vary according to the Cerrado formation, ranging from different grassland formations (*Campo limpo)*, savannah intermediary formations *(Campo sujo*, *Campo cerrado, and Cerrado sensu stricto* - s.s) and forest formations (*Cerradão*).
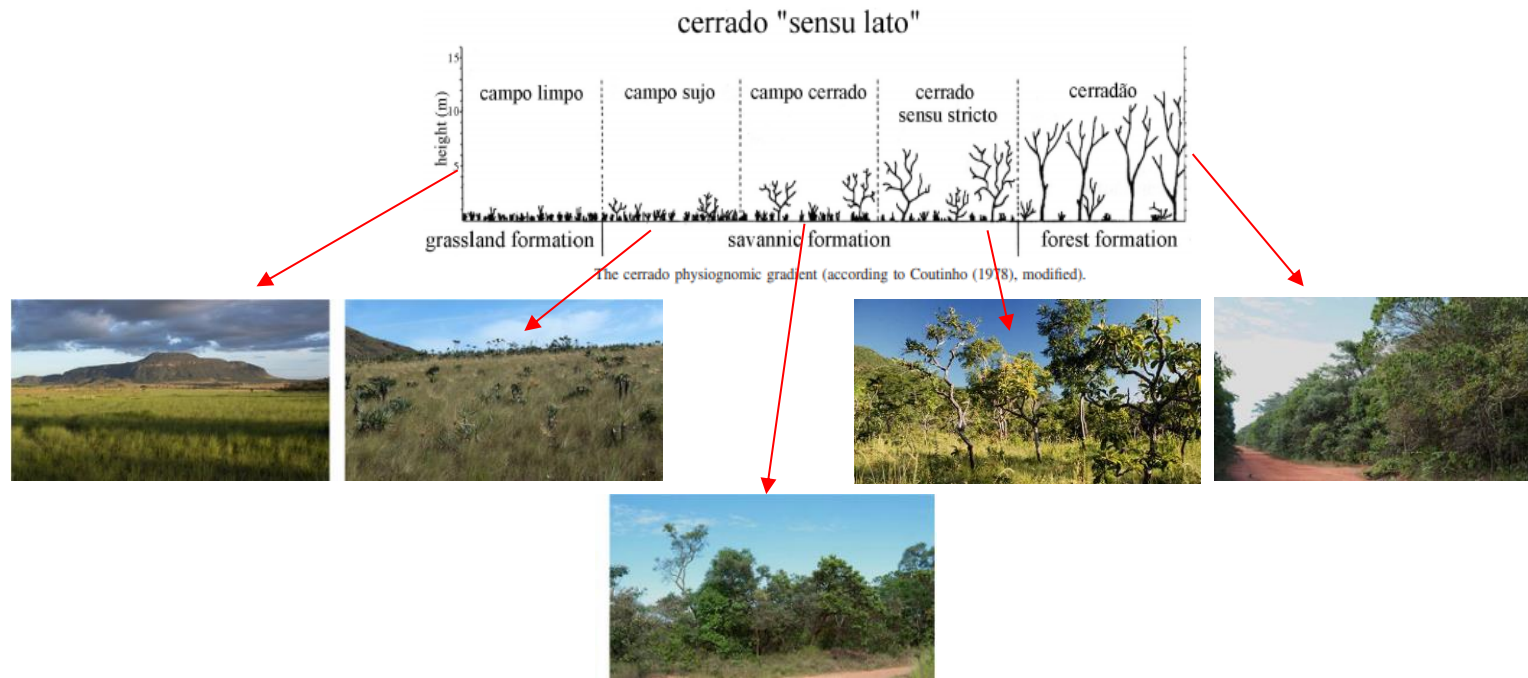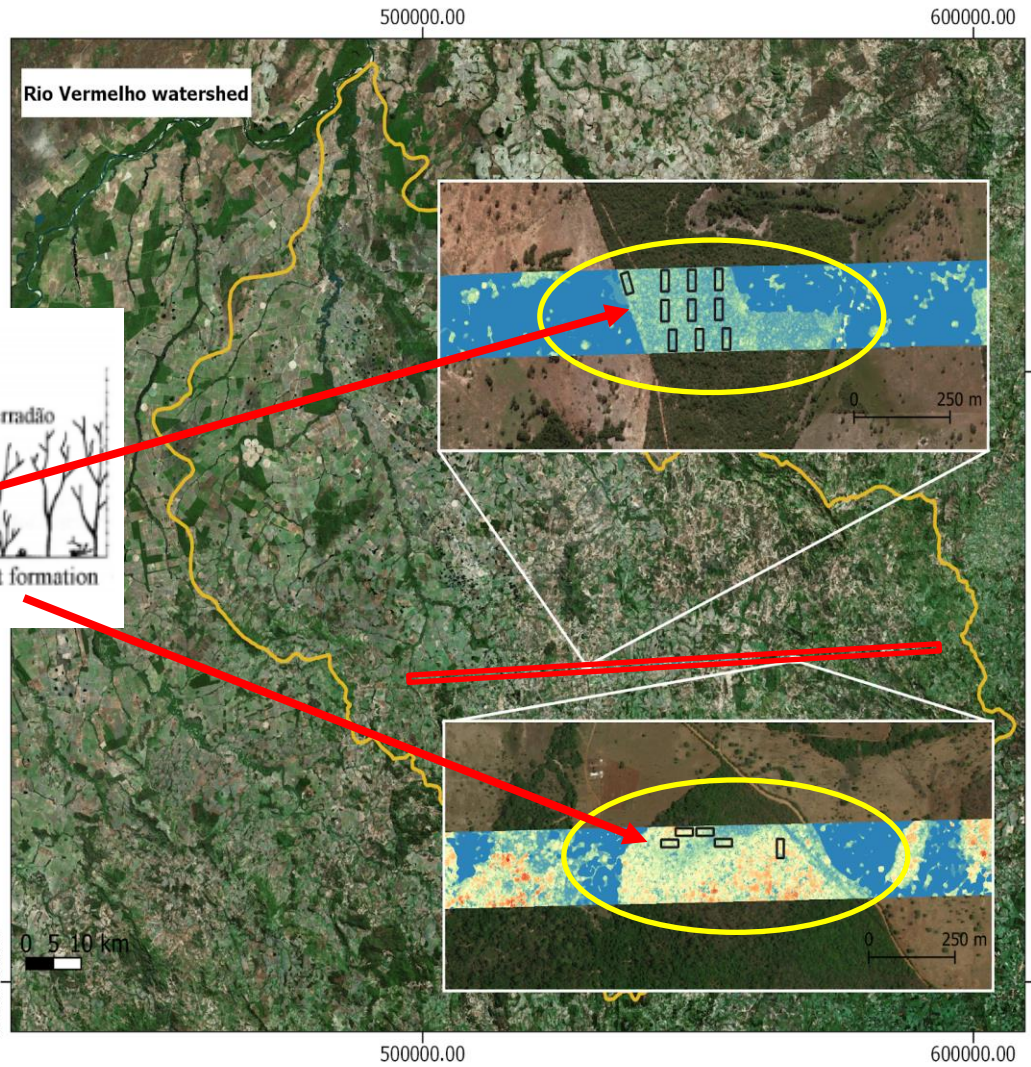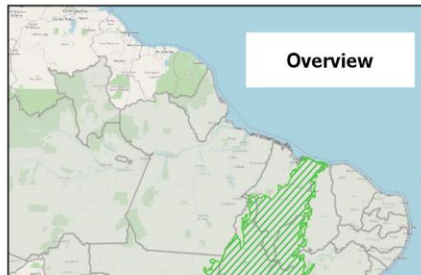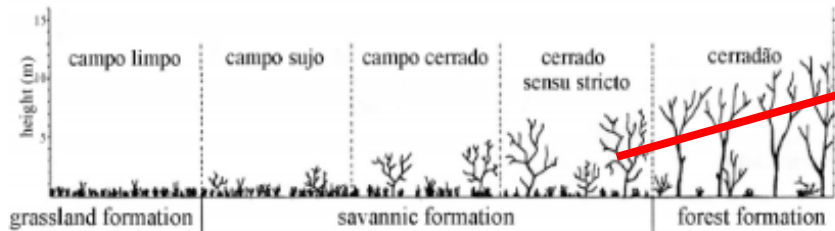
The cerrado physiognomic gradient (according to Coutinho (1978), modified).

Study site

The cerrado physiognomic gradient (according to Coutinho (1978), modified).
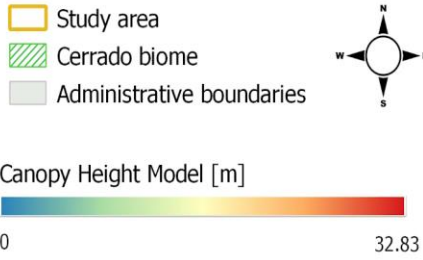
Reference data

- Field data consisted of 15 plots (20mx50m) under the LiDAR footprint.
- AGB was estimated using Scolforo et al. (2008) allometries
- Vegetation structure parameters such as the canopy height model (CHM), canopy density (CD), and canopy cover (CC), were derived from the LiDAR footprint.
- The selected model (R^2 = 0.93, RMSE = 13%) was used to predict AGB across the whole LiDAR flight footprint.

$$AGB \sim -61.92 + 4.88*CHM + 0.83*CC$$

Bispo, et al. 2020, Remote Sensing https://doi.org/10.3390/rs12172685

Rio Vermelho watershed

Clementino area (**CT**)
10 plots (20mX50m)
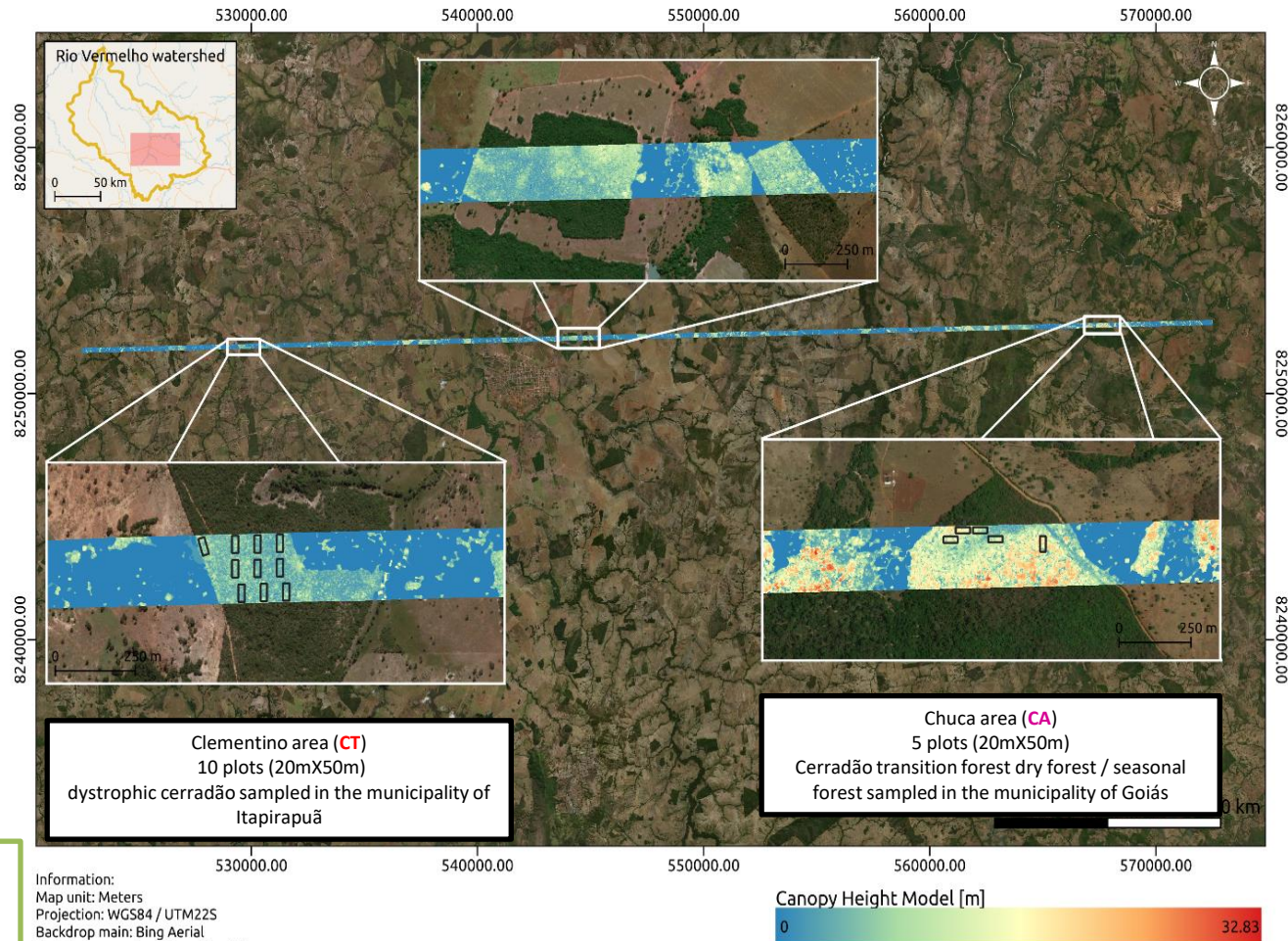dystrophic cerradão sampled in the municipality of Itapirapuã

Chuca area (**CA**)
5 plots (20mX50m)
Cerradão transition forest dry forest / seasonal forest sampled in the municipality of Goiás

Information:
Map unit: Meters
Projection: WGS84 / UTM22S
Backdrop main: Bing Aerial
Backdrop overview: OpenStreetMap
Produced by: University of Leicester
Date: 06.11.2019

Canopy Height Model [m]

0   32.83

LiDAR data obtained rom the Sustainable Landscapes Project by the Brazilian Enterprise for Agricultural Research - EMBRAPA

$$\varepsilon_{AGB} = (\varepsilon_{measurement}^2 + \varepsilon_{allometry}^2 + \varepsilon_{sampling}^2 + \varepsilon_{prediction}^2)^{1/2}$$
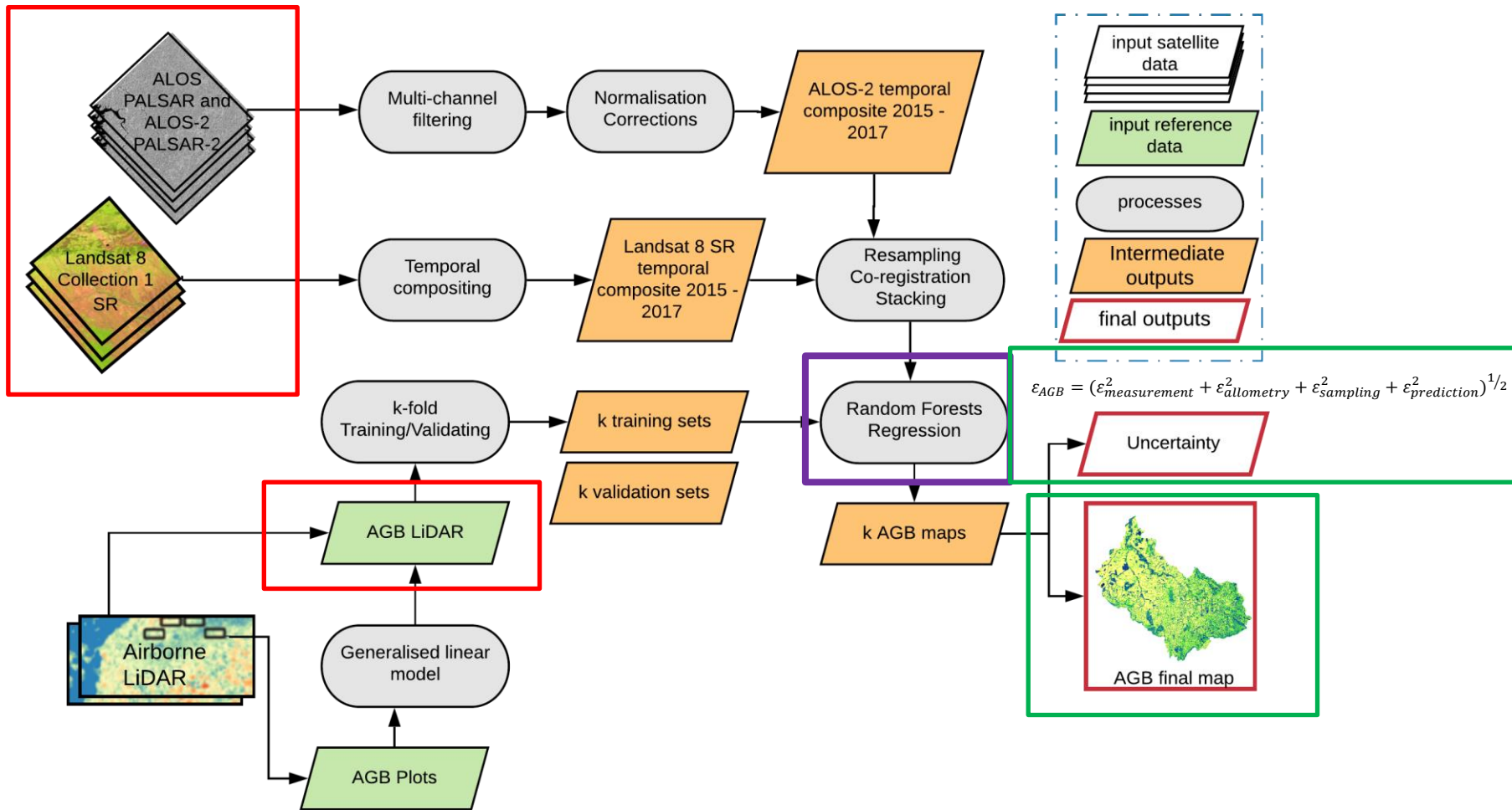
Variable importance analysis
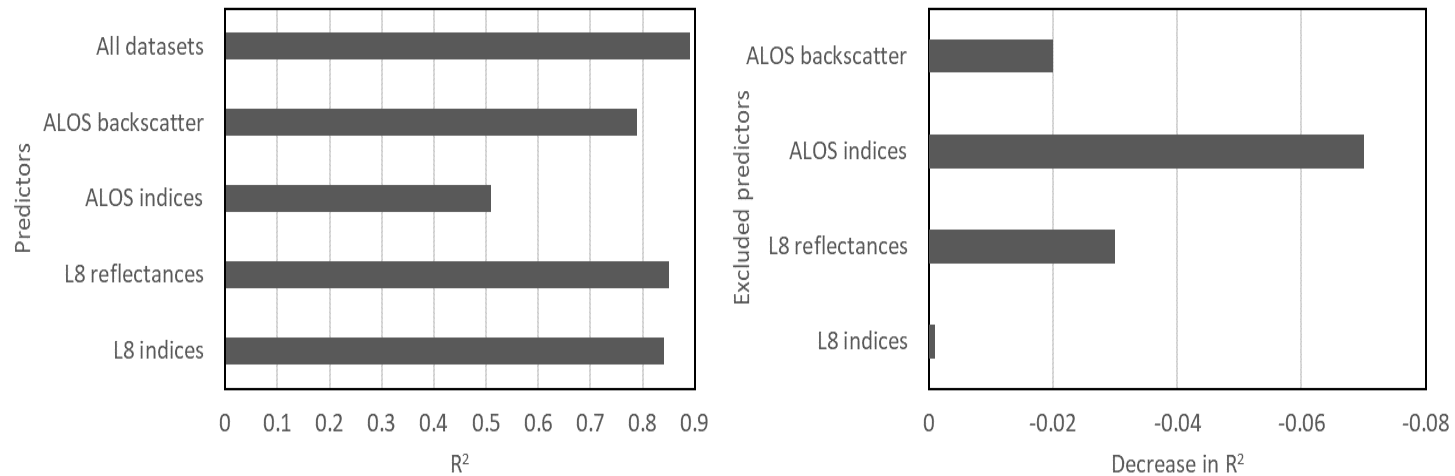
Averaged variable importance analysis across the k-fold procedure for each set of variables derived from Landsat 8 (L8) and ALOS-2/PALSAR-2 (ALOS) included in the RF model. The R^2 for each single set of variables and all variables together (left), and decrease in R^2 for models excluding a single set of variables (right). ALOS backscatter: γ^0_{HV}, γ^0_{HH}. ALOS indices: RFDI, CpR. L8 reflectances: blue, green, red, near infrared, shortwave infrared-1, shortwave infrared-2. L8 indices: NDVI, NBR, NBR2, NDMI, and SAVI.

Cross-validation

$R^2 = 0.89$
RMSE = 7.58 Mg ha^{-1}
Bias = 0.43 Mg ha^{-1}
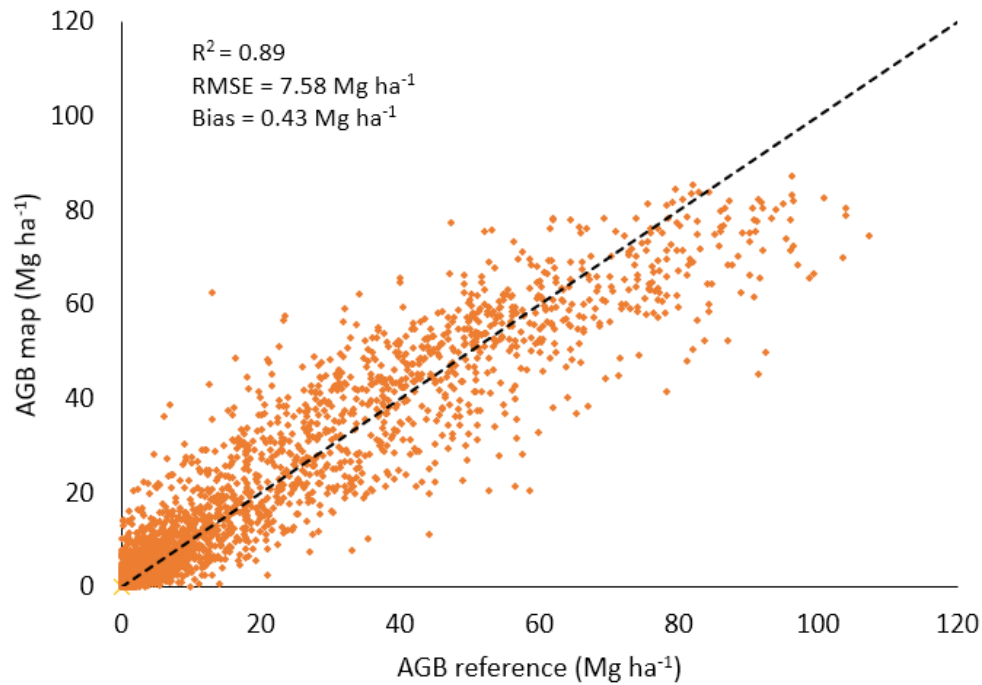
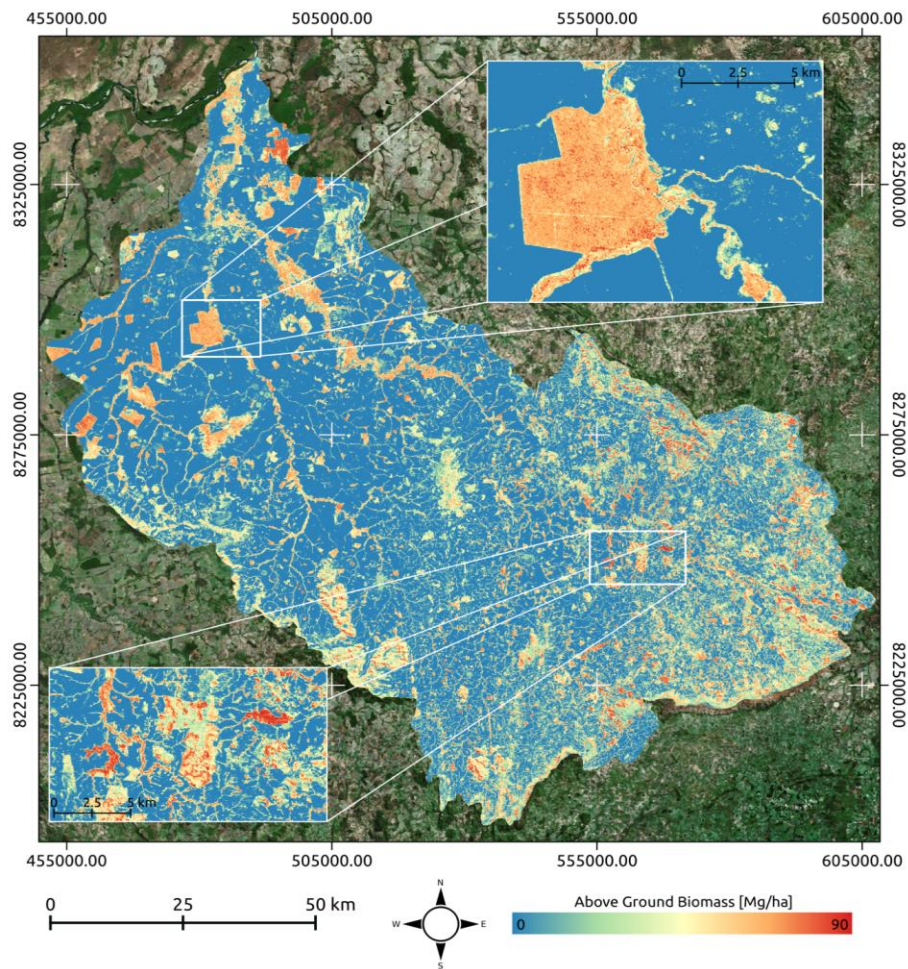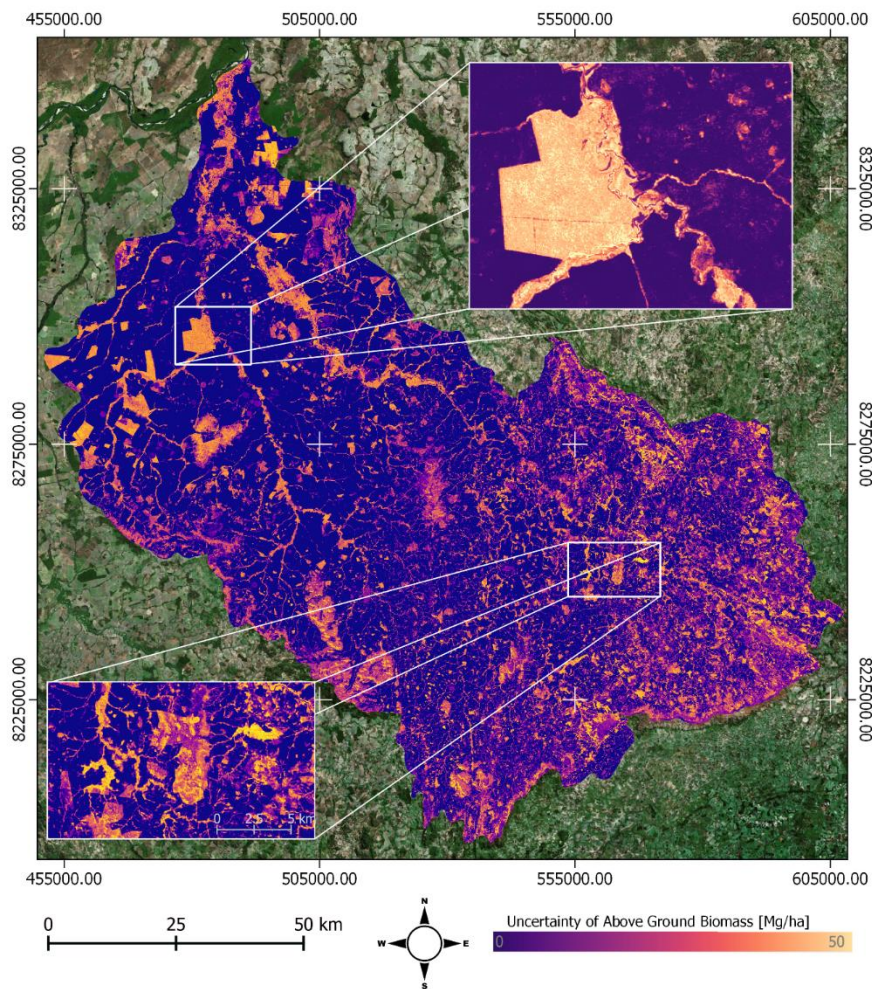Cross-validation between the AGB map predictions and AGB reference data derived from the LiDAR point clouds. The black dash line corresponds to the y = x line.

Bispo, et al. 2020, Remote Sensing https://doi.org/10.3390/rs12172685

AGB

Uncertainty

Above Ground Biomass [Mg/ha]
0 — 90

Uncertainty of Above Ground Biomass [Mg/ha]
0 — 50
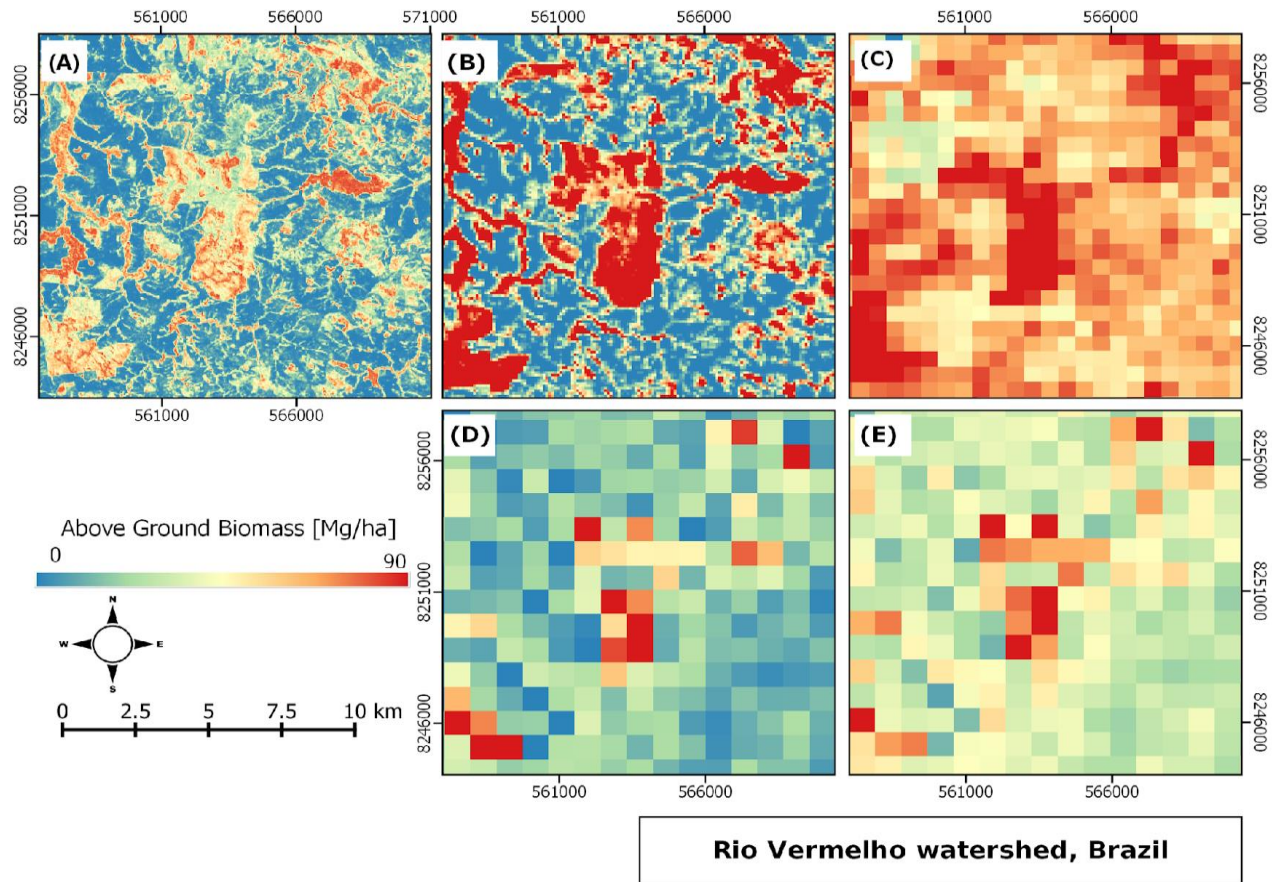
AGB maps over part of the Rio Vermelho watershed, Goiás State, Brazil, produced by this study (30 m) (A) and by Santoro *et al.* *2018* (100 m) (B); Baccini *et al.* 2012 (500m) (C); Avitable *et al*. 2016 (1 km) (D); and Saatchi *et al.* 2011 (1 km) (E).

Wildfires: Penetration through thick smoke can provide more accurate and timely information about the extent of a forest fire and can help quantify vegetation loss.
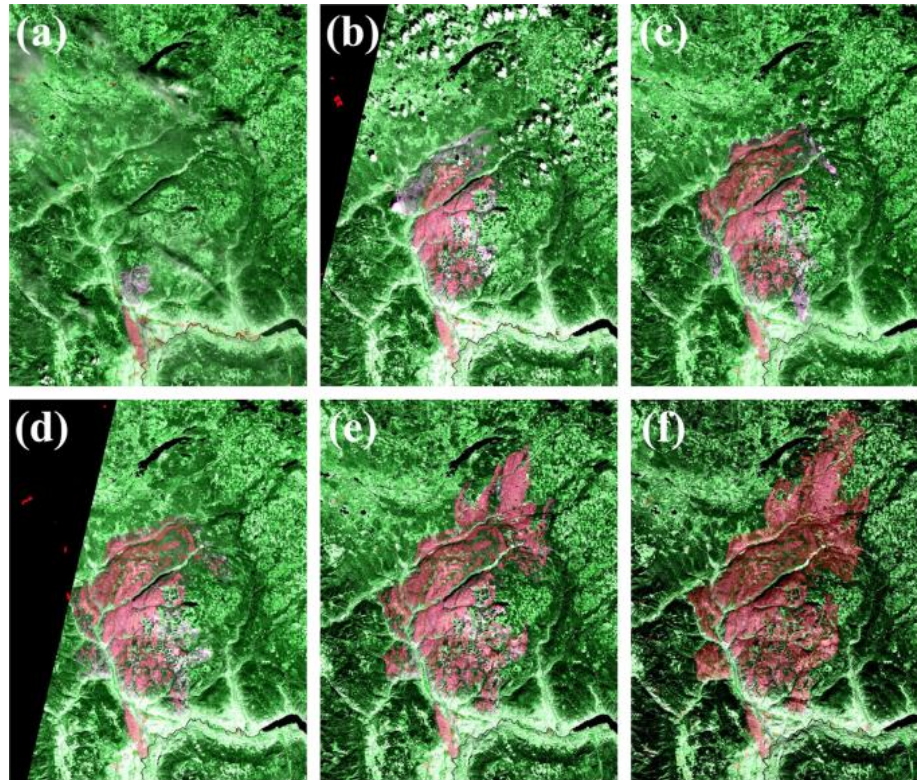
Sentinel-1 based wildfire progression maps in the Elephent Hill (CNN_mrg in transparent red) overlaid on the Sentinel-2 MSI false color composites (R = SWIR2, G = SWIR1, B = SWIR2). (a) SAR-July 8 on MSI-July 10. (b) SAR-July 20 on MSI-July 30. (c) SAR-Aug. 1 on MSI-Aug. 4. (d) SAR-Aug. 8 on MSI-Aug. 11. (e) SAR-Aug. 21 on MSI-Aug. 22. (f) SAR-Sept. 18 on MSI-Oct. 3. The images were generated using Google Earth Engine platform (Map data: Google, ESA).

Ban, Y., Zhang, P., Nascetti, A., Bevington, A.R. and Wulder, M.A., 2020. Near real-time wildfire progression monitoring with Sentinel-1 SAR time series and deep learning. Scientific Reports, 10(1), pp.1-15.

Wetlands: Penetration through wetland areas can reveal flooded vegetation where land is covered by shallow water.

NON-WETLAND
- Barren Land
- Deciduous Forest
- Coniferous Forest

WETLAND
Herbaceous
Moss/Lichen
- Palustrine
Emergent
- Estuarine
- Lacustrine
- Riverine
- Palustrine

Woody
Scrub/Shrub
- Estuarine
- Palustrine
Forested
- Estuarine
- Palustrine

Non-vegetated
- Open water

Wetlands: Penetration through wetland areas can reveal flooded vegetation where land is covered by shallow water.

Dry
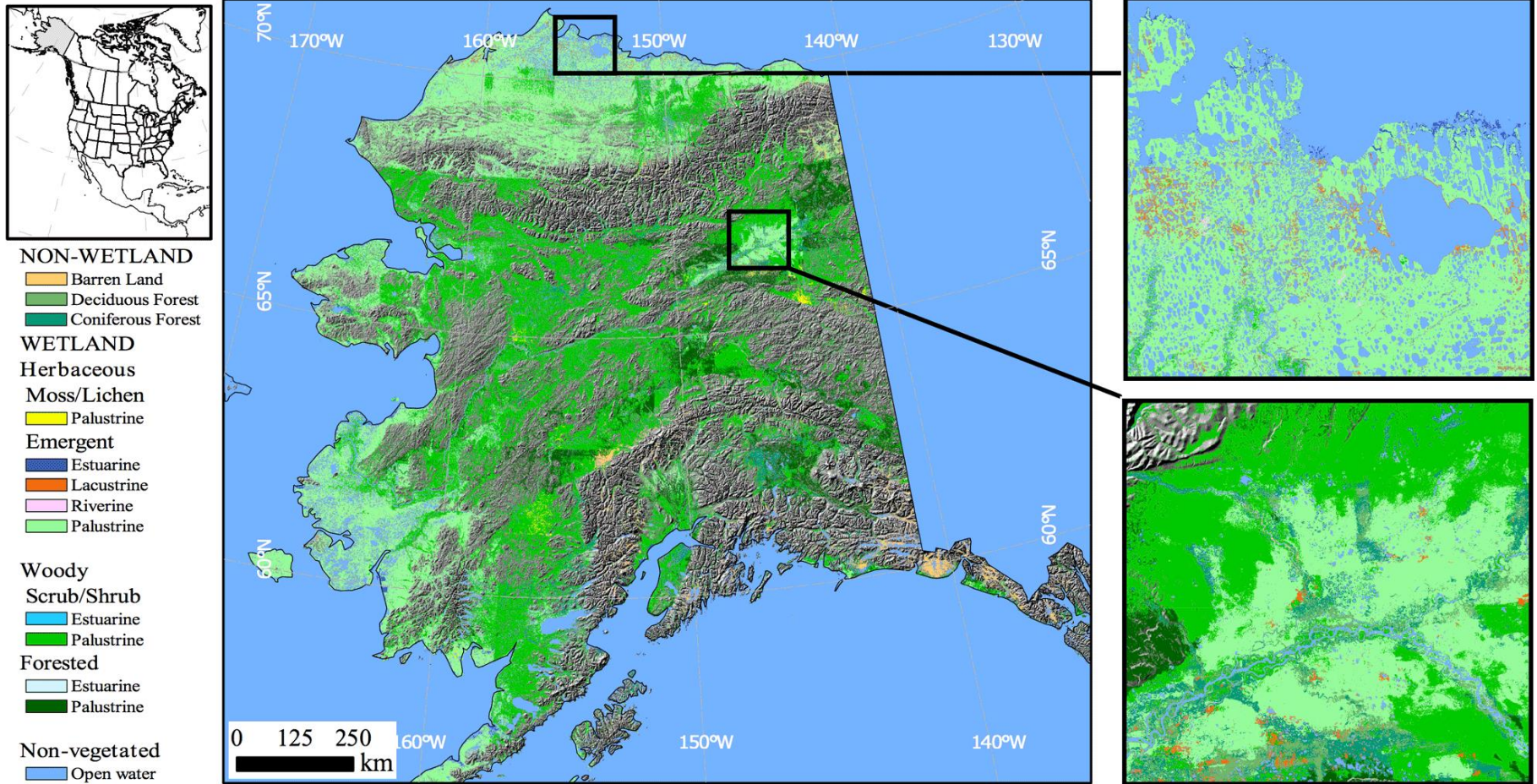
Flood

L – band
C – band
① volume scattering
② specular reflection
③ double bounce
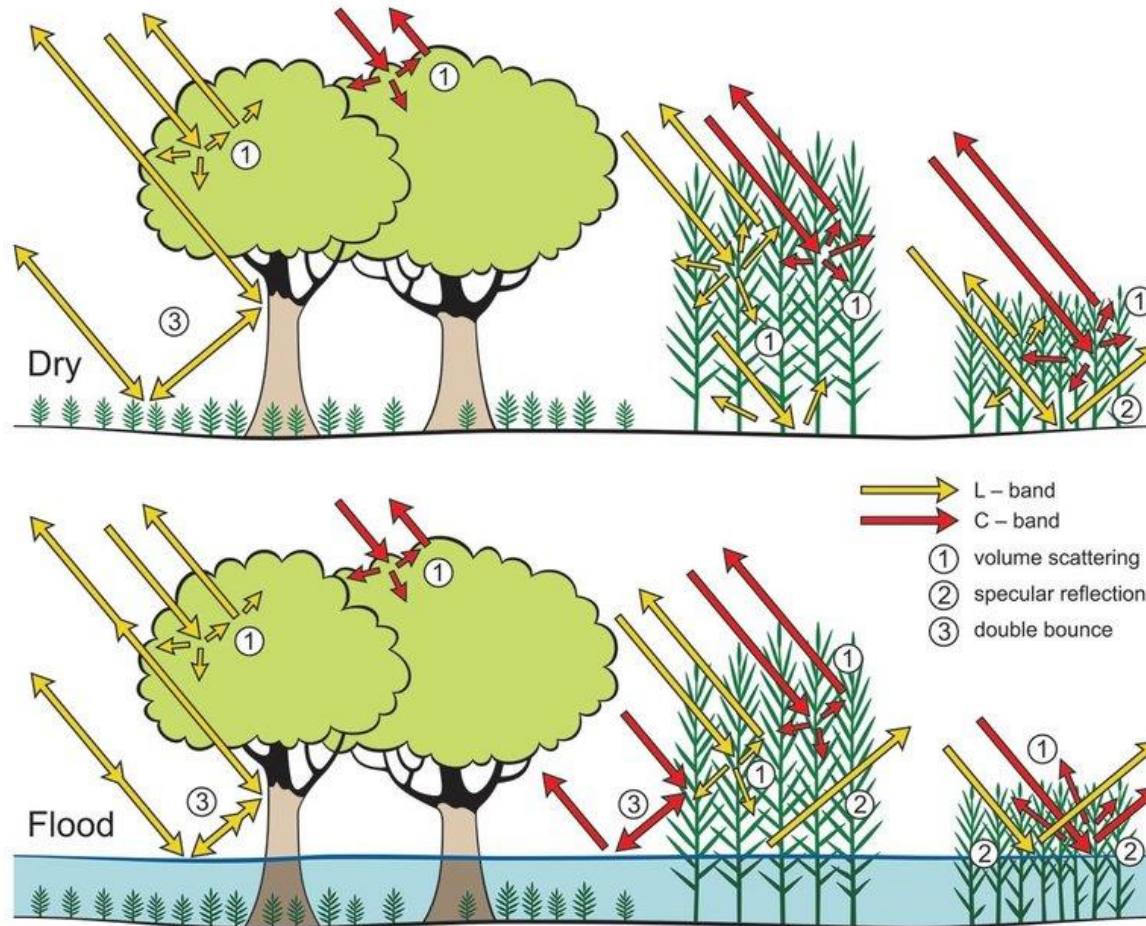
1: C and L-band SAR interactions in tropical wetlands | Download Scientific Diagram (researchgate.net)

Evans, T.L., 2013. *Habitat mapping of the Brazilian Pantanal using synthetic aperture radar imagery and object based image analysis*. University of Victoria (Canada).
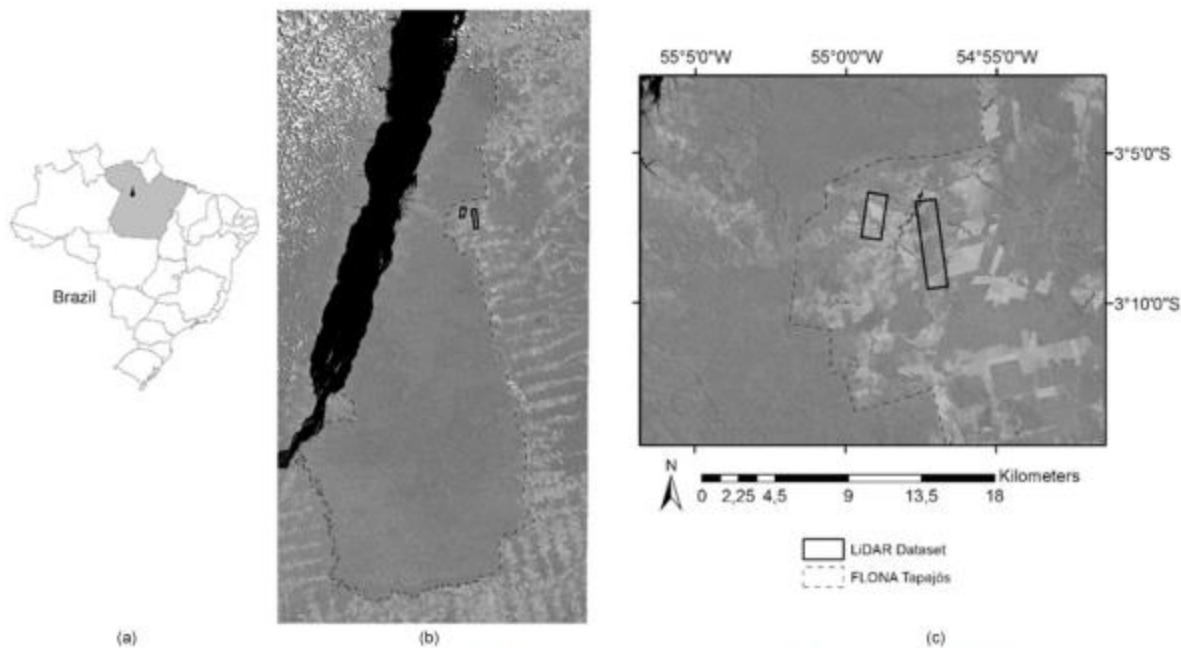
Fig. 1. (a) Location of the TNF in the Brazilian territory. (b) Zoom on the TNF, enclosed by the dashed line (TNF limits from 2013). The two small rectangles delimit the area covered by the LiDAR acquisition. (c) Zoom on the LiDAR coverage. The whole area inside and outside of the two LiDAR rectangles is covered by each TanDEM-X acquisition used in this study (2012, 2013 and 2016). Background image: Landsat 8 (14/08/2015).
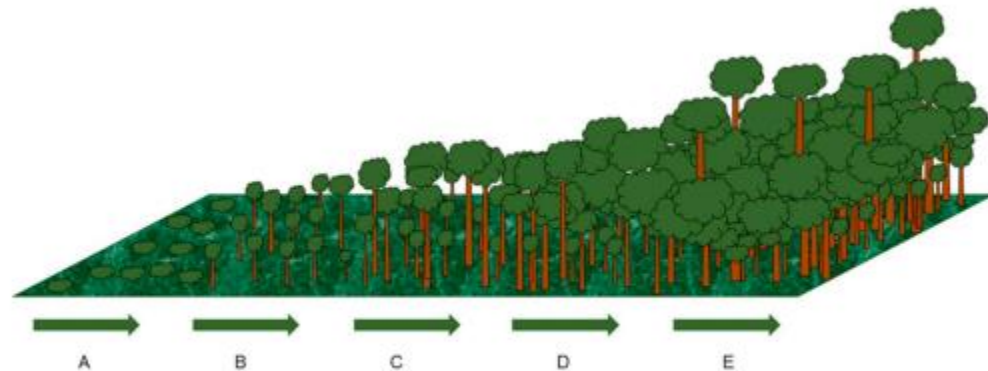

Fig. 2. Schematic representation of a tropical forest with different successional stages: A (non-forest); B (secondary forest in initial stage - SFIni); C (secondary forest in intermediated stage - SFInt); D (secondary forest in advanced stage - SFAdv): E (old growth forest or primary forest - OF).
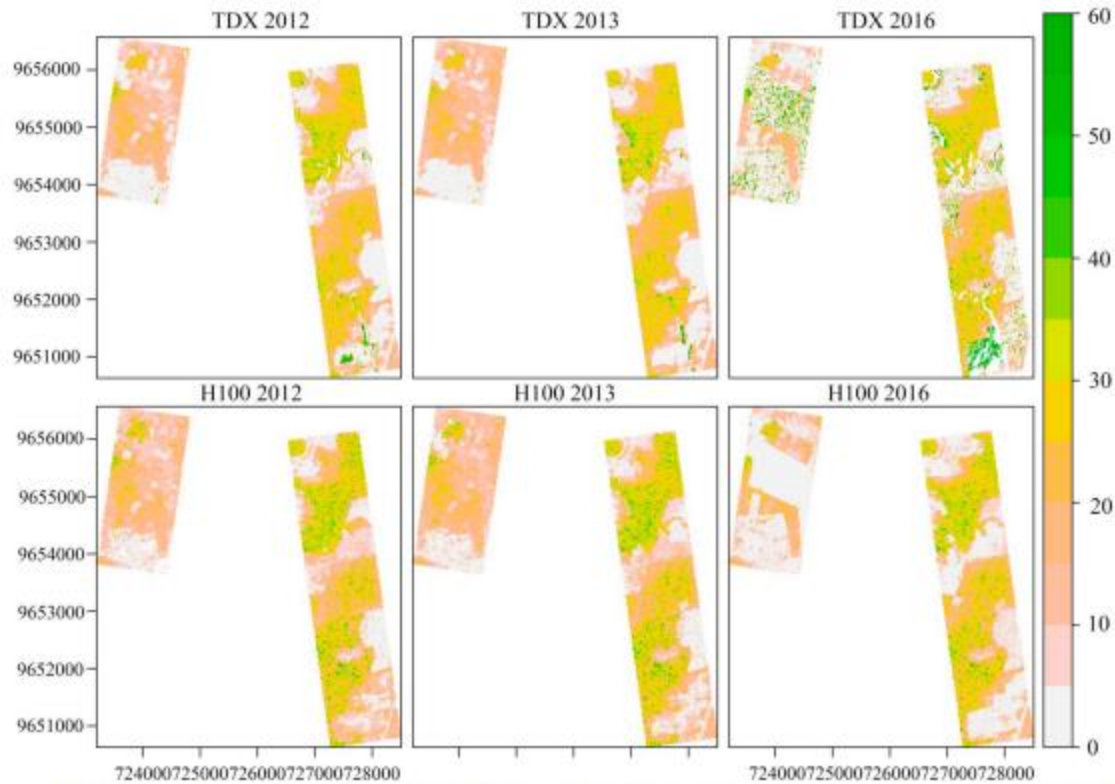
Bispo, P.C. et al., 2019. *Mapping forest successional stages in the Brazilian Amazon using forest heights derived from TanDEM-X SAR interferometry, Remote Sensing of Environment* https://doi.org/10.1016/j.rse.2019.05.013

Fig. 6. Interferometric heights derived from TanDEM-X (top panel) and H100 (bottom panel) derived from LiDAR CHM, for 2012, 2013 and 2016. For each year and sensor, the two rectangles correspond to the LiDAR coverage.
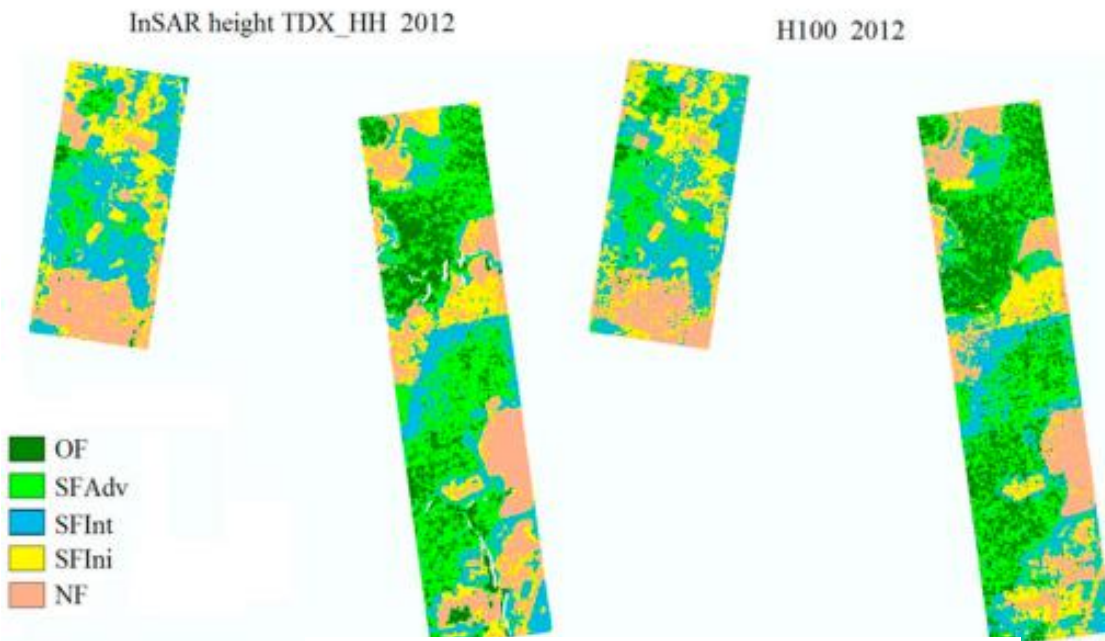
Bispo, P.C. et al., 2019. *Mapping forest successional stages in the Brazilian Amazon using forest heights derived from TanDEM-X SAR interferometry, Remote Sensing of Environment* https://doi.org/10.1016/j.rse.2019.05.013

InSAR height TDX_HH 2012

H100 2012

Fig. 9. Supervised classification of interferometric heights from TanDEM-X HH (05/12/2012) and LiDAR H100 (31/07/2012). The selected classes were old growth forest (OF), secondary forest in advanced stage (SFAdv), secondary forest in intermediary stage (SFInt), secondary forest in initial stage (SFIni) and non-forest (NF). The two rectangles correspond to the LiDAR coverage.

- OF
- SFAdv
- SFInt
- SFIni
- NF

Table 12
Confusion matrix and cross-validation of TanDEM-X and H100 for 2012.

Classes	Ref. OF	Ref. SFAdv	Ref. SFInt	Ref. SFIni	Ref. NF
H100%					
OF	96	3	0	0	0
SFAdv	4	87	8	0	1
SFInt	0	10	83	1	0
SFIni	0	0	9	98	4
NF	0	0	0	1	95
	100	100	100	100	100
Overall Accuracy = 0.92; Kappa = 0.90					
TDX HH%					
OF	93	2	0	0	0
SFAdv	7	84	9	0	0
SFInt	0	14	79	6	0
SFIni	0	0	12	85	1
NF	0	0	0	9	99
	100	100	100	100	100
Overall Accuracy = 0.87; Kappa = 0.84					

Bispo, P.C. et al., 2019. *Mapping forest successional stages in the Brazilian Amazon using forest heights derived from TanDEM-X SAR interferometry, Remote Sensing of Environment* https://doi.org/10.1016/j.rse.2019.05.013

Case Studies: Radar vision in the mapping of forest biodiversity from space | Nature Communications

Radar vision in the mapping of forest biodiversity from space

Soyeon Bae [1*], Shaun R. Levick [2,3], Lea Heidrich[1], Paul Magdon [4], Benjamin F. Leutner [5], Stephan Wöllauer [6], Alla Serebryanyk[7], Thomas Nauss [6], Peter Krzystek[7], Martin M. Gossner [8], Peter Schall[9], Christoph Heibl [10], Claus Bässler[10,11], Inken Doerfler[11,12], Ernst-Detlef Schulze[13], Franz-Sebastian Krah [14,10], Heike Culmsee [15], Kirsten Jung [16], Marco Heurich[10,17], Markus Fischer[18,19], Sebastian Seibold [11,1], Simon Thorn [1], Tobias Gerlach[20], Torsten Hothorn[21], Wolfgang W. Weisser [11] & Jörg Müller [1,10]

Recent progress in remote sensing provides much-needed, large-scale spatio-temporal information on habitat structures important for biodiversity conservation. Here we examine the potential of a newly launched satellite-borne radar system (Sentinel-1) to map the biodiversity of twelve taxa across five temperate forest regions in central Europe. We show that the sensitivity of radar to habitat structure is similar to that of airborne laser scanning (ALS), the current gold standard in the measurement of forest structure. Our models of different facets of biodiversity reveal that radar performs as well as ALS; median R^2 over twelve taxa by ALS and radar are 0.51 and 0.57 respectively for the first non-metric multidimensional scaling axes representing assemblage composition. We further demonstrate the promising predictive ability of radar-derived data with external validation based on the species composition of birds and saproxylic beetles. Establishing new area-wide biodiversity monitoring by remote sensing will require the coupling of radar data to stratified and standardized collected local species data.

61

Case Studies: Near Real-Time Wildfire Progression Monitoring with Sentinel-1 SAR Time Series and Deep Learning | Scientific Reports (nature.com)

SCIENTIFIC REPORTS

natureresearch

OPEN

Near Real-Time Wildfire Progression Monitoring with Sentinel-1 SAR Time Series and Deep Learning

Yifang Ban[1,4*], Puzhao Zhang[1,4*], Andrea Nascetti[1], Alexandre R. Bevington[2] & Michael A. Wulder[3]

In recent years, the world witnessed many devastating wildfires that resulted in destructive human and environmental impacts across the globe. Emergency response and rapid response for mitigation calls for effective approaches for near real-time wildfire monitoring. Capable of penetrating clouds and smoke, and imaging day and night, Synthetic Aperture Radar (SAR) can play a critical role in wildfire monitoring. In this communication, we investigated and demonstrated the potential of Sentinel-1 SAR time series with a deep learning framework for near real-time wildfire progression monitoring. The deep learning framework, based on a Convolutional Neural Network (CNN), is developed to detect burnt areas automatically using every new SAR image acquired during the wildfires and by exploiting all available pre-fire SAR time series to characterize the temporal backscatter variations. The results show that Sentinel-1 SAR backscatter can detect wildfires and capture their temporal progression as demonstrated for three large and impactful wildfires: the 2017 Elephant Hill Fire in British Columbia, Canada, the 2018 Camp Fire in California, USA, and the 2019 Chuckegg Creek Fire in northern Alberta, Canada. Compared to the traditional log-ratio operator, CNN-based deep learning framework can better distinguish burnt areas with higher accuracy. These findings demonstrate that spaceborne SAR time series with deep learning can play a significant role for near real-time wildfire monitoring when the data becomes available at daily and hourly intervals with the launches of RADARSAT Constellation Missions in 2019, and SAR CubeSat constellations.

Case Studies: [Remote Sensing | Free Full-Text | Change Detection of Selective Logging in the Brazilian Amazon Using X-Band SAR Data and Pre-Trained Convolutional Neural Networks (mdpi.com)](#)

Open Access   Article

Change Detection of Selective Logging in the Brazilian Amazon Using X-Band SAR Data and Pre-Trained Convolutional Neural Networks

by Tahisa Neitzel Kuck [1,2] ✉ ⓘ, Paulo Fernando Ferreira Silva Filho [1] ✉ ⓘ, Edson Eyji Sano [2,3] ✉ ⓘ, Polyanna da Conceição Bispo [4,*] ✉ ⓘ, Elcio Hideiti Shiguemori [1] ✉ ⓘ and Ricardo Dalagnol [4,5] ✉ ⓘ

[1] Command, Control, Communications, Computers, Intelligence, Surveillance and Reconnaissance Division, Institute for Advanced Studies (IEAv), São José dos Campos 12228-001, Brazil

[2] Geoscience Institute, Universidade de Brasília (UnB), Brasília 70910-900, Brazil

[3] Embrapa Cerrados, Planaltina 73310-970, Brazil

[4] Department of Geography, School of Environment, Education and Development, University of Manchester, Manchester M13 9PL, UK

[5] Earth Observation and Geoinformatics Division, National Institute for Space Research-INPE, São José dos Campos 12227-010, Brazil

* Author to whom correspondence should be addressed.
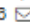
View Full-Text   **Download PDF**   **Browse Figures**   **Citation Export**

Case Studies: Remote Sensing | Free Full-Text | Discriminating Forest Successional Stages, Forest Degradation, and Land Use in Central Amazon Using ALOS/PALSAR-2 Full-Polarimetric Data (mdpi.com)

Discriminating Forest Successional Stages, Forest Degradation, and Land Use in Central Amazon Using ALOS/PALSAR-2 Full-Polarimetric Data

by Natalia C. Wiederkehr [1,*], Fabio F. Gama [1], Paulo B. N. Castro [2], Polyanna da Conceição Bispo [3], Heiko Balzter [4,5], Edson E. Sano [6], Veraldo Liesenberg [7], João R. Santos [1] and José C. Mura [1]

[1] National Institute for Space Research, Av. dos Astronautas, 1.758, São José dos Campos, São Paulo 12227-010, Brazil

[2] Campus Universitário, Federal University of Ouro Preto, Morro do Cruzeiro, Ouro Preto, Minas Gerais 35400-000, Brazil

[3] Department of Geography, School of Environment, Education and Development, University of Manchester, Oxford Road, Manchester M13 9PL, UK

[4] Centre for Landscape and Climate Research (CLCR), University of Leicester, Bennett Building, University Road, Leicester LE1 7RH, UK

[5] National Center for Earth Observation, University of Leicester, Michael Atiyah Building, University Road, Leicester LE1 7RH, UK

[6] Embrapa Cerrados, BR-020, Planaltina, Federal District 73310-970, Brazil

[7] Forest Engineering Department, Santa Catarina State University, Avenida Luiz de Camões 2090, Lages, Santa Catarina 88520-000, Brazil

* Author to whom correspondence should be addressed.

View Full-Text   Download PDF   Browse Figures   Citation Export
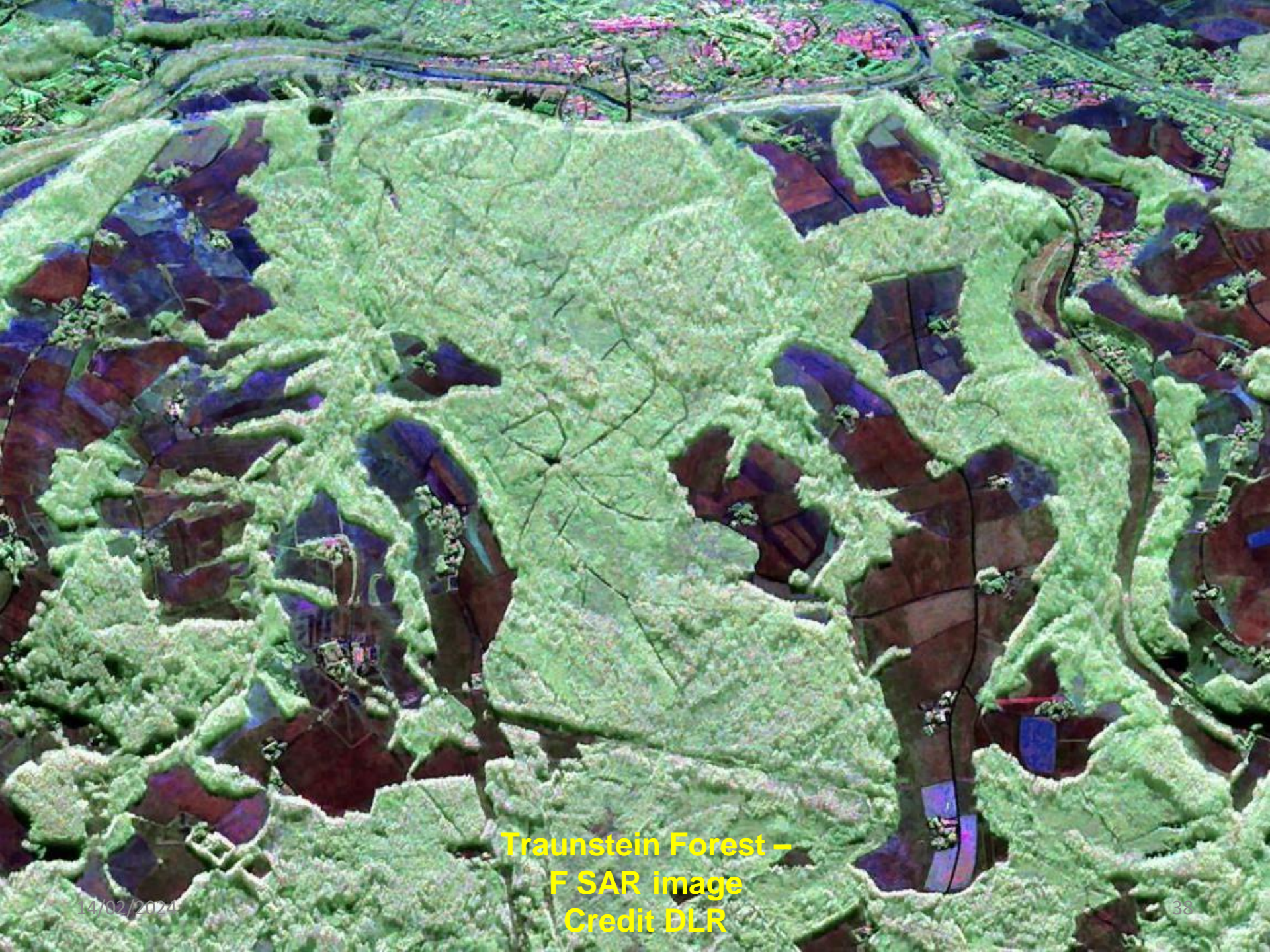
Traunstein Forest –
F SAR image
Credit DLR